Sulfur and lead isotopic compositions of massive sulfides from deep-sea hydrothermal systems: Implications for ore genesis and fluid circulation

Zhigang Zeng [a,b,c,d,*], Yao Ma [a,c], Shuai Chen [a], David Selby [e], Xiaoyuan Wang [a,b], Xuebo Yin [a]

[a] Seafloor Hydrothermal Activity Laboratory of the Key Laboratory of Marine Geology and Environment, Institute of Oceanology, Chinese Academy of Sciences, Qingdao 266071, China
[b] Laboratory for Marine Mineral Resources, Qingdao National Laboratory for Marine Science and Technology, Qingdao 266071, China
[c] University of Chinese Academy of Sciences, Beijing 100049, China
[d] Qingdao Collaborative Innovation Center of Marine Science and Technology, Qingdao 266071, China
[e] Department of Earth Sciences, University of Durham, Durham DH1 3LE, UK

ABSTRACT

Studies of sulfur and lead isotopic compositions in hydrothermal deposits are an important tool to determine the source and processes of both sulfur and lead, and to understand the origin of hydrothermal ore deposits. Here, the sulfur and lead isotopic compositions of sulfide minerals have been studied for different hydrothermal fields in the East Pacific Rise (EPR), Mid-Atlantic Ridge (MAR), Central Indian Ridge (CIR), Southwest Indian Ridge (SWIR), and North Fiji Basin (NFB). The sulfur isotopic compositions of the studied sulfide samples are variable ($\delta^{34}S$ 0.0 to 9.6‰, avg. $\delta^{34}S$ 4.7‰; n = 60), being close to the associated igneous rocks (~0‰ for, e.g., basalt, serpentinized peridotite), which may reflect the S in the sulfide samples is derived mainly from the associated igneous rocks, and a relatively small proportion (<36%) of seawater sulfur incorporated into these sulfides during mixing between seawater ($\delta^{34}S$ 21‰) and hydrothermal fluid. In contrast for a mixed origin for the source of S, the majority of the lead isotopic compositions ($^{206}Pb/^{204}Pb$ 17.541 ± 0.004 to 19.268 ± 0.001, $^{207}Pb/^{204}Pb$ 15.451 ± 0.001 to 15.684 ± 0.001, $^{208}Pb/^{204}Pb$ 37.557 ± 0.008 to 38.988 ± 0.002, n = 21) of the sulfides possess a basaltic Pb isotopic composition, suggesting that the lead in the massive sulfide is mainly leached from local basaltic rocks that host the sub-seafloor hydrothermal systems in sediment-free mid-ocean ridges and mature back-arc basins. Furthermore, sulfide minerals in the super-fast and fast spreading mid-ocean ridges (MORs) exhibit less spread in their the $\delta^{34}S$ values compared to sulfides from super-slow, and slow spreading MORs, which is most easily explained as a lesser degree of fluid-rock interaction and hydrothermal fluid-seawater mixing during hydrothermal ore-forming process. Additionally, the S and Pb isotope compositions of sulfides are controlled by the fluid processes for forming seafloor massive sulfide deposits. We demonstrate that the variable sulfur and lead isotopic compositions exhibit a relationship with the sulfur and lead sources, fluid–rock interaction, and fluid–seawater mixing.

© 2016 Elsevier B.V. All rights reserved.

1. Introduction

Sulfur (S) and lead (Pb) isotopes are powerful tracers for exploring seafloor hydrothermal processes, fluid-rock interaction, and magmatic activity, in order to interpret the origin of hydrothermal ore deposits, in particular the sources of S and Pb in sulfide minerals (e.g., Shanks and Niemitz, 1982; Fouquet and Marcoux, 1995; Ohmoto and Goldhaber, 1997; Bjerkgård et al., 2000; Hannington et al., 2005; Kim et al., 2006; Seal, 2006; Yao et al., 2009; Zeng et al., 2010; Aoyama et al., 2014; McDermott et al., 2015). The S and Pb isotope characteristics of massive sulfide deposits from modern seafloor hydrothermal systems in mid-ocean ridges (MORs) and back-arc basins (BABs) have been summarized by Halbach et al. (1989, 1997), Fouquet and Marcoux (1995), Verati et al. (1999), Seal et al. (2000), Zeng et al. (2000a, 2000b), Shanks (2001), Cousens et al. (2002), Kim et al. (2004, 2006), Hannington et al. (2005), and Yao et al. (2009).

Sulfur isotopic values of seafloor hydrothermal sulfides indicate that the sulfur is most likely derived from multiple sources: (1) seawater sulfate ($\delta^{34}S$ ~21‰); (2) igneous-rock-derived sulfur ($\delta^{34}S$ ~0‰), including mid-ocean ridge basalt, mantle peridotites, and calc-alkaline volcanic rocks (e.g., andesites, rhyolites); (3) magmatic sulfur derived from magmatic degassing (e.g., $\delta^{34}S$ −5‰ of sulfides from the Hine Hina field in the Lau basin; Herzig et al., 1998a); and (4) bacteriogenic

sulfide from sediments (e.g., Ohmoto and Rye, 1979; Shanks et al., 1981, 1995; Shanks and Niemitz, 1982; Solomon et al., 1988; Peter and Shanks, 1992; Herzig et al., 1998a). For sediment-starved MORs, the variation in the sulfur isotopic composition of the sulfides is explained by varying proportions of reduced seawater sulfate and mantle-derived sulfur leached from the underlying igneous rocks (e.g., Arnold and Sheppard, 1981; Herzig et al., 1998a). In contrast, for sediment-associated MORs, negative sulfur isotope values generally occur along with low sulfide-sulfur contents and can be caused by bacterial sulfate reduction (Goldhaber and Kaplan, 1980; Brunner and Bernasconi, 2005). Furthermore, because the equilibrium fractionation between H_2S and sulfides is limited at temperature ≥250 °C, variation in the $\delta^{34}S$ values of sulfides can be interpreted as temporal variations in the $\delta^{34}S$ values of H_2S in the hydrothermal fluids (Styrt et al., 1981; Bluth and Ohmoto, 1988). However, the variation in the $\delta^{34}S_{H2S}$ values could have been caused by the variation in $\delta^{34}S_{\Sigma S}$, the pH and redox state (i.e., SO_4^-/H_2S ratio), or by the degree of sulfur isotopic equilibrium between SO_4^{2-} species and H_2S species in the fluid (Ohmoto and Rye, 1979). It is also unlikely that kinetic isotopic effects played an important role in the variation of $\delta^{34}S$ values of vent fluids and hydrothermal sulfides (Bluth and Ohmoto, 1988). Therefore, the variation in sulfur isotopic compositions of hydrothermal sulfides might be due to changes in the end-member fluid composition, in-situ sulfate reduction, or local disequilibrium sulfur isotopic fractionation during sulfide deposition (Fouquet et al., 1996). In addition, the $\delta^{34}S$ values of sulfides essentially reflect the isotope fractionation factor between sulfate (SO_4) and sulfide (H_2S) (Ohmoto et al., 1983; Ohmoto and Goldhaber, 1997), and the isotope fractionation factors between SO_4 and H_2S are 21‰ and 15‰ at 300 and 400 °C, respectively (Ohmoto and Lasaga, 1982). For the sulfur isotope system, Farquhar et al. (2003) and Johnston et al. (2005a) demonstrated that bacterial sulfate reduction follows a mass-dependent relationship that is measurably different (i.e., $^{33}\alpha = {}^{34}\alpha^{0.512}$) from that expected from thermochemical equilibrium (i.e., $^{33}\alpha = {}^{34}\alpha^{0.515}$). As a result, natural samples can show measurable and systematic variations in $\Delta^{33}S$ ($= \delta^{33}S - 0.515 \times \delta^{34}S$) as well as $\Delta^{36}S$ ($= \delta^{36}S - 1.90 \times \delta^{34}S$) even when $\delta^{34}S$ values are identical (Ono et al., 2006). In the Lau basin, isotopically light sulfur ($\delta^{34}S$ −5‰), which is observed in the sulfides from the Hine Hina field, may be produced in several ways, including biogenic reduction of seawater SO_4, fractionation of sulfur between reduced and oxidized species as a result of large shifts in the oxidation state of the fluids (e.g., by boiling), or by the evolution of light sulfur directly from a magmatic volatile phase (Herzig et al., 1998a).

Furthermore, in the Trans-Atlantic Geotraverse (TAG) hydrothermal field, the range of sulfur isotopic compositions of sulfides is significantly larger (4.4 to 8.9‰) than that of sulfides from the EPR near 21°N and 13°N, which has been interpreted to suggest that the TAG hydrothermal massive sulfides formed as a result of multiple-stages of hydrothermal activity (Stepanova et al., 1996; Knott et al., 1998). In addition, on the EPR near 21°N, the $\delta^{34}S$ values of the late-stage pyrite samples, which appear to infill fluid conduits, are among the lowest observed, suggesting precipitation in the fluid conduits of sulfide deposits isolated from seawater influx or perhaps at temperatures below 200–250 °C, above which sulfate reduction becomes rapid (Shanks et al., 1981; Ohmoto and Lasaga, 1982; Woodruff and Shanks, 1988).

Lead isotopic compositions of seafloor hydrothermal sulfides indicate that the lead is most likely derived from three sources: (1) basalts at MORs (e.g., Brévart et al., 1981; LeHuray et al., 1988; Fouquet and Marcoux, 1995; Zeng et al., 2010); (2) sediments at BABs (e.g., Halbach et al., 1997; Zeng et al., 2000b) and MORs (e.g., LeHuray et al., 1988; Zierenberg et al., 1993; Cousens et al., 2002); (3) volcanic rocks that have inherited lead from the subducted slab, including basalt and its sediment at BABs (Fouquet and Marcoux, 1995; Kim et al., 2004). On sediment-starved ridges, the Pb in hydrothermal sulfides is considered to have been mobilized from the volcanic crust during hydrothermal circulation based on the sulfide Pb isotope compositions that are indistinguishable from that of the local basalt (e.g., Brévart et al., 1981;

Vidal and Clauer, 1981; LeHuray et al., 1988; Fouquet and Marcoux, 1995; Andrieu et al., 1998; Zeng et al., 2010). The Pb isotopic compositions of the sulfides are also more homogeneous than the adjacent volcanic rocks, suggesting that the Pb isotopes have been homogenized during hydrothermal circulation, and that the contribution of Pb from seawater and hemipelagic sediments is very low (e.g., Brévart et al., 1981; Vidal and Clauer, 1981; Chen, 1987; Hegner and Tatsumoto, 1987; LeHuray et al., 1988; Fouquet and Marcoux, 1995; Andrieu et al., 1998; Charlou et al., 2002; Yao et al., 2009; Zeng et al., 2010).

Furthermore, on sediment-covered MORs, such as the Middle Valley on the Juan de Fuca Ridge, the Escanaba Trough in the Gorda Ridge, and the Guaymas Basin in the Gulf of California, the Pb in the seafloor hydrothermal sulfides is considered to have been sourced from both the mid-ocean ridge basalt (MORB) and the sediment (LeHuray et al., 1988; Goodfellow and Franklin, 1993). In this setting, the sulfides possess a larger range and more radiogenic compositions due to a contribution of lead from the pelagic and terrigenous sediments, in addition to basalt lavas, through which the hydrothermal fluids have passed (e.g., LeHuray et al., 1988; Zierenberg et al., 1993; German et al., 1995; Stuart et al., 1999; Bjerkgård et al., 2000; Cousens et al., 1995, 2002,).

In contrast to the Pb isotopic compositions of sulfides from sediment-starved MORs, the Pb isotopic characteristics of seafloor hydrothermal sulfides in the Jade hydrothermal field of the Okinawa Trough are distinctly different, which can be interpreted as a mixture of roughly equal parts of volcanic lead with lead derived from the Okinawa Trough sediments (Halbach et al., 1997; Zeng et al., 2000b). The Pb of hydrothermal sulfides in the chimneys in the Eastern Manus Basin has been leached from the surrounding andesite and dacite during hydrothermal circulation, and the slightly more radiogenic Pb isotope composition of the Susu knolls sulfides compared to those from PACMANUS, indicate that the Susu knolls site is possibly affected more by an arc component than the PACMANUS site (Kim et al., 2004). In the North Fiji Basin, the Pb of hydrothermal sulfides in chimneys is from MORB, and the formation of chimneys was possibly related to E-MORB volcanism (Kim et al., 2006). In the Lau Basin, the Pb of seafloor hydrothermal sulfides is from three end-member sources: basalts from the Pacific Ocean and Indian Ocean plates, and pelagic sediments (Fouquet and Marcoux, 1995).

In this paper, we present the first results of S and Pb isotope analyses of massive sulfides from the EPR near 1–2°S, the MAR near 13°S, the CIR at Kairei hydrothermal field (KHF), Edmond hydrothermal field (EHF) at 25°S, and the Southwest Indian Ridge (SWIR) in area A (Fig. 1). In addition, $\delta^{34}S$ and Pb isotope analyses were performed on the massive sulfides from the EPR near 13°N and 11°N, the MAR at the Logatchev hydrothermal field (LHF), and the North Fiji BAB at the Sonne 99 hydrothermal field (S99HF) (Fig. 1). The main purposes of the paper are: (1) to investigate the characteristics of the S and Pb isotope compositions of sulfides from the EPR near 1–2°S, the MAR near 13°S, the CIR at KHF, EHF, and the SWIR in area A; (2) to characterize the sources of S and Pb; and (3) to understand the effect of fluid-rock interaction, fluid–seawater mixing, magmatic activity, and spreading rate of MORs on the S and Pb isotopic compositions of massive sulfides.

2. Geological setting and sample mineralogy

Seafloor hydrothermal sulfide samples were recovered by TV-grab samplers from the fast-spreading EPR near 13°N, the ultra-fast spreading EPR near 1–2°S, the Kairei hydrothermal field (KHF), the Edmond hydrothermal field (EHF) on the intermediate-spreading CIR near 25°S, the slow-spreading MAR near 13°S, the LHF (15°N), the ultra-slow spreading SWIR near 63.5°E and in area A (49°E) in 2005, 2007, 2008, 2009, and 2010 during the DY105-17, DY115-19, DY115-20, and DY115-21 cruises of R/V Dayang Yihao. Sulfide samples from the Sonne 99 hydrothermal field (S99HF) in the back-arc North Fiji Basin (NFB) were collected in 1998 during the SO134 cruise of HYFIFLUX II (Fig. 1).
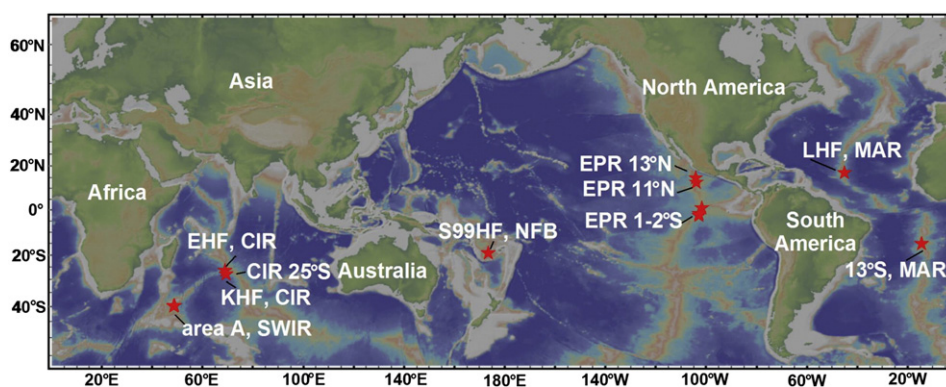
Fig. 1. Locations of seafloor hydrothermal sulfide samples from deep-sea hydrothermal fields analyzed for sulfur and lead isotopic compositions in this study. KHF–Kairei hydrothermal field; EHF–Edmond hydrothermal field; CIR–Central Indian Ridge; SWIR–Southwest Indian Ridge; S99HF–Sonne 99 hydrothermal field; NFB–North Fiji Basin; EPR–East Pacific Rise; LHF–Logatchev hydrothermal field; MAR–Mid-Atlantic Ridge.

At the EPR near 13°N, 11°N, and 1–2°S, the KHF, EHF, the MAR near 13°S, the area A, and the S99HF, the seafloor hydrothermal sulfides are hosted by mid-ocean ridge basalts (MORBs) (e.g., Kumagai et al., 2008; Zeng et al., 2010, 2014, 2015a, 2015b). The KHF is situated on basaltic rocks, but the hydrothermal fluids also interact with and circulate through ultramafic rocks (Nakamura et al., 2009). In the LHF, the hydrothermal sulfide deposit is associated with ultramafic rocks located in a debris flow consisting of heterogeneous ultramafic and mafic intrusive rocks, including serpentinized harzburgite, serpentinized dunite, gabbronorite, and olivine-bearing basalt (e.g., Petersen et al., 2009; Zeng et al., 2014, 2015a, 2015b). In addition, in the North Fiji Basin, the S99HF is located immediately south of the triple junction point at 16°50′S and is hosted by basaltic rocks, the trace element composition of which indicates that magma generation was influenced by two different sources: normal mid-ocean ridge basalt (N-MORB) and ocean island basalt (OIB)- related to enriched mid-ocean ridge basalt (E-MORB) (Eissen et al., 1994; Nohara et al., 1994; Koschinsky et al., 2002; Kim et al., 2006).

3. Samples and analytical methods

3.1. Sampling procedures

Table 1 and Fig. 1 show the sampling location, depth, and mineralogy of the hydrothermal sulfide samples. Seafloor hydrothermal sulfide samples consist of major pyrite ± marcasite, chalcopyrite, sphalerite, anhydrite, barite, and amorphous silica. Sulfide mineral aggregate samples were taken from different seafloor hydrothermal sulfide deposits. Samples denoted as pyrite, sphalerite, and chalcopyrite + pyrite consist of abundant (>30%) pyrite, sphalerite, and chalcopyrite + pyrite, respectively. All samples for S and Pb isotope analysis were crushed and sieved to select sulfide aggregates between >1 mm and 1 cm. All sample chips were crushed with an agate mortar and pestle and sieved to select sulfide grains between 50 μm and 2 mm in size (Zeng et al., 2014, 2015a, 2015b). The sulfides were separated from non-sulfide minerals, e.g., sulfates and amorphous silica, via ethanol elutriation (Zeng et al., 2014, 2015a, 2015b). This purification of the sulfide aliquots by ethanol elutriation is based on specific gravity and uses a stream of ethanol that flows counter to the direction of grain flow in a glass dish. The less dense particles rise to the top (overflow) because their terminal grain velocities are lower than the velocity of the rising fluid. Because most of the samples were fine-grained and intergrown, an integrated mechanical separating method was used to obtain a monomineralic sulfide or mineral aggregate. The separation methods included a high-frequency dielectric splitter, magnetic separator, and electromagnetic separator (Zeng et al., 2014, 2015a, 2015b). All sulfide samples were then carefully picked manually under a binocular microscope to avoid sulfates and oxides, and were ultrasonically cleaned in ultrapure alcohol to remove any seawater influences, e.g., the presence of salts and altered seawater products. Then, all the

samples were ground to a powder finer than 63 μm in an agate mortar (Zeng et al., 2014, 2015a, 2015b). Fine-grained glass powder was used as an abrasive to polish the mortar and pestle between samples to exclude cross- contamination. In addition, one sulfate sample was also prepared by hand picking and was similarly prepared for sulfur isotopic analysis.

3.2. Analytical methods

Sulfide samples (<0.1 mg) were combusted in a tin cup using a modified Roboprep elemental analyzer attached to a Finnigan 252 mass spectrometer at the Environmental Isotopes Pty Ltd., Macquarie Center, NSW 2113, Australia. V_2O_5 was added to the sulfate samples and standards to enhance combustion. Samples were analyzed relative to an internal gas standard and laboratory standards (Ag$_2$S-3, $\delta^{34}S = +0.4‰$ VCDT and CSIRO-S-SO$_4$, $\delta^{34}S = +20.4‰$ VCDT). The laboratory standards had been calibrated using international standards IAEA-S1 ($\delta^{34}S = -0.3‰$ VCDT) and NBS-127 ($\delta^{34}S = +20.3‰$ VCDT). Replicate analyses of sulfide standards were within $\pm 0.2‰$.

Lead abundances were measured on separate 40-mg splits of powdered sulfide aggregates. These pretreated samples were digested in vials by using 0.5 mL of 22.5 mol/L HF, 2 mL of 12 mol/L HCl and 0.7 mL of 16 mol/L HNO$_3$ (all acids at metal-oxide-semiconductor pure grade) at 150 °C for 24 h in closed Teflon vials on an electrothermal hotplate. Then, 0.2 mL of 12.4 mol/L HClO$_4$ was added, and the samples were dried at 120 °C until no white smoke was present. When the samples were almost dry, 1 mL of 16 mol/L HNO$_3$ and 1 mL of deionized Milli-Q water (18.2 MΩ cm resistivity) were added, and the mixture was re-heated in closed vials on the hotplate at 120 °C for 12 h (Yin et al., 2011). Finally, Pb was analyzed by an IRIS Intrepid II XSP ICP-AES (Thermoelectricity Company) at the Qingdao Institute of Marine Geology. The reference materials GBW07267, GBW07268, GBW07270, and WMS-1A were run as external standards to evaluate the accuracy. The relative standard deviation (RSD), which was calculated from standard reference materials, was <2%.

Between 100 and 200 mg of powdered sulfide aggregates were dissolved in 50% HF-12 N HNO$_3$, then treated with 8 N HNO$_3$ and finally 6 N HCl. The residue was taken up in 1 N HBr, and Pb was separated on Bio-Rad 10-mL polyethylene columns and Dowex AG1-8X anion resin, using 6 N HCl to elute Pb. The collected Pb solution was dried and redissolved in 1 N HBr, and the above procedure was repeated with a small-volume resin bed. Samples were loaded onto single Re filaments with H$_3$PO$_4$ and silica gel and were analyzed at the Department of Earth Sciences, Carleton University, with a Triton Tl thermal ionization mass spectrometer. Total procedural blanks for Pb were <450 pg. The average ratios measured for NBS 981 were $^{206}Pb/^{204}Pb = 16.888 \pm 0.007$, $^{207}Pb/^{204}Pb = 15.425 \pm 0.009$, and $^{208}Pb/^{204}Pb = 36.492 \pm 0.030$. One duplicate run of sample 19III-S12-TVG6 showed good agreement between the two results (Table 4).

Table 1
Description of seafloor massive sulfide samples for sulfur and lead isotopic compositions in this study.

Field	Sample no.	Latitude	Longitude	Water depth (m)	Basement rocks	Description	Sulfide mineralogy
Ultra-fast spreading mid-ocean ridge							
1–2°S, EPR	20III-S4-TVG1-1-1	1°22.130′S	102°37.360′W	2747	Basalts	Porous chimney fragment coated with tan Fe hydroxides and partially filled conduits	Py+++; Mc+, Cpy+; Sp+
1–2°S, EPR	20III-S4-TVG1-1-2	1°22.130′S	102°37.360′W	2747	Basalts	Porous chimney fragment coated with tan Fe hydroxides and partially filled conduits	Py+++; Mc+, Cpy+; Sp+
1–2°S, EPR	20III-S4-TVG1-1-3	1°22.130′S	102°37.360′W	2747	Basalts	Porous chimney fragment coated with tan Fe hydroxides and partially filled conduits	Py+++; Mc+, Cpy+; Sp+
1–2°S, EPR	20III-S4-TVG1-1-4	1°22.130′S	102°37.360′W	2747	Basalts	Porous chimney fragment coated with tan Fe hydroxides and partially filled conduits	Py+++; Mc+, Cpy+; Sp+
1–2°S, EPR	20III-S4-TVG1-2-1	1°22.130′S	102°37.360′W	2747	Basalts	Chimney fragment coated with tan Fe hydroxides	Py+++, Cpy++; Mc++; Sp+
1–2°S, EPR	20III-S4-TVG1-2-2	1°22.130′S	102°37.360′W	2747	Basalts	Chimney fragment coated with tan Fe hydroxides	Py+++, Cpy++; Mc++; Sp+
1–2°S, EPR	20III-S4-TVG1-2-3	1°22.130′S	102°37.360′W	2747	Basalts	Chimney fragment coated with tan Fe hydroxides	Py+++, Cpy++; Mc++; Sp+
1–2°S, EPR	20III-S6-TVG3	2°09.102′S	102°38.760′W	2921	Basalts	Outer chimney wall fragment coated with red brown Fe hydroxides and white anhydrite layer	Mc+++, Py+++; Sp++; Cpy+
1–2°S, EPR	21III-S17-TVG13	0°50.226′S	101°27.954′W	2899	Basalts	Outer chimney wall fragment coated with red brown Fe hydroxides and white anhydrite layer	Mc+++, Py+++; Sp++; Cpy+
Fast-spreading mid-ocean ridge							
13°N, EPR	EPR05-TVG1-2-1	12°42.669′N	103°54.426′W	2628	Basalts	Fe-rich massive sulfides coated with tan Fe hydroxides, and small conduits	Py+++; Sp+, Cpy+
13°N, EPR	EPR05-TVG1-2-2	12°42.669′N	103°54.426′W	2628	Basalts	Fe-rich massive sulfides coated with tan Fe hydroxides, and small conduits	Py+++; Sp+, Cpy+
13°N, EPR	EPR05-TVG1-2-4	12°42.669′N	103°54.426′W	2628	Basalts	Fe-rich massive sulfides coated with tan Fe hydroxides, and small conduits	Py+++; Sp+, Cpy+
13°N, EPR	EPR05-TVG1-2-2	12°42.669′N	103°54.426′W	2628	Basalts	Fe-rich massive sulfides coated with tan Fe hydroxides, and small conduits	Py+++; Sp+, Cpy+
13°N, EPR	EPR05-TVG1-3-2	12°42.669′N	103°54.426′W	2628	Basalts	Fe-rich massive sulfides coated with tan Fe hydroxides, and oxidized pyrite aggregates	Py+++; Cpy+, Sp+
13°N, EPR	EPR05-TVG1-3-3	12°42.669′N	103°54.426′W	2628	Basalts	Fe-rich massive sulfides coated with tan Fe hydroxides, and oxidized pyrite aggregates	Py+++; Cpy+, Sp+
13°N, EPR	EPR05-TVG2-1-1	12°42.678′N	103°54.414′W	2633	Basalts	Fe-rich massive sulfides coated with tan Fe hydroxides and many elliptical cavities, showing development of mineral zoning	Py+++, Mc+++; Sp+
13°N, EPR	EPR05-TVG2-1-2	12°42.678′N	103°54.414′W	2633	Basalts	Fe-rich massive sulfides coated with tan Fe hydroxides and many elliptical cavities, showing development of mineral zoning	Py+++, Mc+++; Sp+
13°N, EPR	EPR05-TVG2-1-4	12°42.678′N	103°54.414′W	2633	Basalts	Fe-rich massive sulfides coated with tan Fe hydroxides and many elliptical cavities, showing development of mineral zoning	Py+++, Mc+++; Sp+
11°N, EPR	1384-2-2	10°56′N	103°41′W	2500	Basalts	Inactive Zn-rich chimney fragment with yellowish-brown Fe oxides and anhydrite, and Cu-rich inner conduit	Zn+++; Py++; Cpy+
Intermediate-spreading mid-ocean ridge							
KHF, CIR	IR05-TVG-9-1	25°19.221′S	70°02.420′E	2437	Basalts	Chimney fragment with finely bladed chalcopyrite	Py+++; Cpy+
KHF, CIR	IR05-TVG-9-2	25°19.221′S	70°02.420′E	2437	Basalts	Chimney fragment with finely bladed chalcopyrite	Py+++; Cpy+
KHF, CIR	IR05-TVG-9-3	25°19.221′S	70°02.420′E	2437	Basalts	Chimney fragment with finely bladed chalcopyrite	Py+++; Cpy+
25°S, CIR	19III-S12-TVG6	25°09.228′S	70°04.482′E	2443	Basalts	Porous Cu-rich sulfide fragment with yellowish brown oxides in the cavities, local light green secondary Cu sulfides	Cpy+++
EHF, CIR	IR05-TVG12-5-2	23°52.678′S	69°35.808′E	3293	Basalts	Grey black Zn-rich massive sulfides coated with red to brown oxide crusts, nodular structure in the outside	Sp+++; Py++, Mc++
EHF, CIR	IR05-TVG12-8-2	23°52.678′S	69°35.808′E	3293	Basalts	Grey black Zn-rich massive sulfides coated with red to brown oxide crusts, nodular structure in the outside	Sp+++; Py++, Mc++
EHF, CIR	IR05-TVG12-8-4	23°52.678′S	69°35.808′E	3293	Basalts	Grey black Zn-rich massive sulfides coated with red to brown oxide crusts, nodular structure in the outside	Sp+++; Py++, Mc++
EHF, CIR	IR05-TVG12-9-1	23°52.678′S	69°35.808′E	3293	Basalts	Grey black Zn-rich massive sulfides coated with red to brown oxide crusts, nodular structure in the outside	Sp+++; Py++, Mc++
EHF, CIR	IR05-TVG12-11	23°52.678′S	69°35.808′E	3293	Basalts	Grey black Zn-rich massive sulfides coated with red to brown oxide crusts, nodular structure in the outside	Sp+++; Py++, Mc++
EHF, CIR	IR05-TVG12-14	23°52.678′S	69°35.808′E	3293	Basalts	Grey black Zn-rich massive sulfides coated with red to brown oxide crusts, nodular	Sp+++; Py++, Mc++

Table 1 (*continued*)

Field	Sample no.	Latitude	Longitude	Water depth (m)	Basement rocks	Description	Sulfide mineralogy
						structure in the outside	
EHF, CIR	IR05-TVG13-4-1	23°52.684′S	69°35.795′E	3292	Basalts	Oxidized columnar chimney coated with red brown oxides, and fluid conduits	Cpy +++; Mc++, Sp ++, Py ++
EHF, CIR	IR05-TVG13-4-2	23°52.684′S	69°35.795′E	3292	Basalts	Oxidized columnar chimney coated with red brown oxides, and fluid conduits	Cpy +++; Mc++, Sp ++, Py ++
EHF, CIR	IR05-TVG13-9.1	23°52.684′S	69°35.795′E	3292	Basalts	Irregular crust consisted of red brown to yellowish green oxide, anhydrite and gypsum, with disseminated sulfides	Py +++
EHF, CIR	IR05-TVG13-9.2–1	23°52.684′S	69°35.795′E	3292	Basalts	Chimney fragment with red, brown and yellowish green mixture of oxide, anhydrite and gypsum	Mc +++; Cpy ++, Sp ++, Py ++
EHF, CIR	IR05-TVG13-9.2–2	23°52.684′S	69°35.795′E	3292	Basalts	Chimney fragment with red, brown and yellowish green mixture of oxide, anhydrite and gypsum	Mc +++; Cpy ++, Sp ++, Py ++
EHF, CIR	19III-S18-TVG9	23°52.638′S	69°35.850′E	3282	Basalts	Porous Fe-Cu rich sulfides with minor sulfates	Py +++; Mc++, Sp ++, Cpy++
Slow-spreading mid-ocean ridge							
LHF, MAR	MAR05-TVG1-9	14°45.186′N	44°58.772′W	3025	Ultramafic rocks	Porous Cu-rich massive sulfide	Cpy +++; Py ++
LHF, MAR	MAR05-TVG1-10-2	14°45.186′N	44°58.772′W	3025	Ultramafic rocks	Fragment with gypsum, amorphous silica, disseminated marcasite and chalcopyrite	Cpy +++; Py ++
LHF, MAR	MAR05-TVG1-10-3	14°45.186′N	44°58.772′W	3025	Ultramafic rocks	Fragment with gypsum, amorphous silica, disseminated marcasite and chalcopyrite	Cpy +++; Py ++
LHF, MAR	MAR05-TVG1-21	14°45.186′N	44°58.772′W	3025	Ultramafic rocks	Cu-rich massive sulfides fragment with small cavities	Cpy +++; Sp +; Py +
13°S, MAR	21IV-S7-TVG4-1	13°17.203′S	14°24.837′W	2311	Basalts	Zn-Fe rich massive sulfide fragment coated with Fe hydroxides and Cu sulfides	Sp +++, Py +++; Cpy +
Ultra-slow spreading mid-ocean ridge							
Area A, SWIR	19II-S7-TVG4	37°47.004′S	49°28.176′E	2781	Basalts	Black porous massive sulfides	Sp +++, Py ++; Cpy +
Area A, SWIR	20V-S34-TVG16	37°46.812′S	49°38.886′E	2780	Basalts	Massive sulfide fragment with dark brown oxide crust	Py +++; Cpy +
Area A, SWIR	20V-S35-TVG17-1-1	37°46.812″S	49°38.886′E	2783	Basalts	Massive sulfide with dark brown oxide crust	Po ++, Py ++; Cpy +
Area A, SWIR	20V-S35-TVG17-3-2	37°46.812″S	49°38.886′E	2783	Basalts	Massive sulfide with dark brown oxide crust	Po ++, Py ++; Cpy +
Area A, SWIR	20V-S35-TVG17-4-1	37°46.812″S	49°38.886′E	2783	Basalts	Massive sulfide with dark brown oxide crust	Po ++, Py ++; Cpy +
Area A, SWIR	20V-S35-TVG17-7	37°46.812″S	49°38.886′E	2783	Basalts	Massive sulfide with dark brown oxide crust	Po ++, Py ++; Cpy +
Area A, SWIR	21VII-TVG22	37°56.316′S	49°15.894′E	1443	Basalts	Fe-rich chimney fragment coated with grey amorphous silica, conduits partially in-filled with oxides	Cpy +++, Py +++; Mc +, Sp +
Back-arc basin							
S99HF, NFB	26.1GTV-1	16°57.602′S	173°54.991′E	1976	Basalts	Inner Zn-rich chimney wall fragment with yellowish brown oxides	Sp +++; Mc +, Cpy +
S99HF, NFB	26.1GTV-2	16°57.602′S	173°54.991′E	1976	Basalts	Inner Zn-rich chimney wall fragment with yellowish brown oxides	Sp +++; Mc +, Cpy +
S99HF, NFB	26.2GTV-1	16°57.602′S	173°54.991′E	1976	Basalts	Greyish Zn-rich chimney fragment with local honeycomb structure and coarse black sphalerite crystals	Sp +++; Mc +, Cpy +
S99HF, NFB	26.2GTV-2	16°57.602′S	173°54.991′E	1976	Basalts	Greyish Zn-rich chimney fragment with local honeycomb structure and coarse black sphalerite crystals	Sp +++; Mc +, Cpy +
S99HF, NFB	26.2GTV-3	16°57.602′S	173°54.991′E	1976	Basalts	Greyish Zn-rich chimney fragment with local honeycomb structure and coarse black sphalerite crystals	Sp +++; Mc +, Cpy +
S99HF, NFB	42GTV-2	16°57.533′S	173°54.978′E	1975	Basalts	Cu-rich chimney fragment with conduits	Cpy +++; Py ++, Mc ++
S99HF, NFB	42GTV-3	16°57.533′S	173°54.978′E	1975	Basalts	Cu-rich chimney fragment with conduits	Cpy +++; Py ++, Mc ++
S99HF, NFB	113.1GTV-1	16°57.322′S	173°54.970′E	1967	Basalts	Porous massive sulfide	Py ++, Cpy ++
S99HF, NFB	113.1GTV-2	16°57.322′S	173°54.970′E	1967	Basalts	Porous massive sulfide	Py ++, Cpy ++
S99HF, NFB	113.1GTV-3	16°57.322′S	173°54.970′E	1967	Basalts	Porous massive sulfide	Py ++, Cpy ++
S99HF, NFB	113.1GTV-4	16°57.322′S	173°54.970′E	1967	Basalts	Porous massive sulfide	Py ++, Cpy ++
S99HF, NFB	113.2GTV	16°57.322′S	173°54.970′E	1967	Basalts	Porous massive sulfide	Py ++, Cpy ++

EPR–East Pacific Rise; KHF–Kairei Hydrothermal Field; EHF–Edmond Hydrothermal Field; CIR–Central Indian Ridge; SWIR–Southwest Indian Ridge; S99HF–Sonne 99 Hydrothermal Field; NFB–North Fiji Basin; LHF–Logatchev Hydrothermal Field; MAR–Mid-Atlantic Ridge. Py–pyrite; Mc–marcasite; Cpy–chalcopyrite; Sp–sphalerite; Po–pyrrhotite. +++: abundant (>30%); ++: major (5–30%); +: minor (≤5%).

4. Results

4.1. Sulfur isotopic compositions in sulfides

Sulfide minerals forming in the EPR near 13°N, 11°N, and 1–2°S, the LHF, the MAR near 13°S, the KHF, the EHF, the CIR near 25°S, area A, and the S99HF exhibit a range of $\delta^{34}S$ values from 0.0 to 9.6‰ (see Table 2; Fig. 2), with an average value of 4.7‰ (n = 60), falling within the overall range of $\delta^{34}S$ values for sulfide samples from other seafloor hydrothermal field (from 1 to 9‰; n = 1841) (Fig. 3). A single value of 21.5‰ for the sulfate sample at the EHF falls within the overall range of sulfate samples from other seafloor hydrothermal fields (from 19 to 25‰; n = 288) (data are from Shanks and Niemitz, 1982; Kerridge et al., 1983; Zierenberg et al., 1984, 1993; Koski et al., 1985; Shanks and Seyfried, 1987; Hannington and Scott, 1988; Zierenberg and Shanks, 1988, 1994; Kusakabe et al., 1990; Blum and Puchelt, 1991; Iizasa et al.,

Table 2
Sulfur isotopic compositions of seafloor hydrothermal sulfide and sulfate minerals from the EPR near 1–2°S, 13°N and 11°N, KHF, CIR near 25°S, EHF, LHF, MAR near 13°S, area A, and S99HF.

Sample no.	Mineralogy	$\delta^{34}S_{VCDT}$ (‰)	Sample no.	Mineralogy	$\delta^{34}S_{VCDT}$ (‰)
1–2°S, EPR			*EHF, CIR*		
20III-S4-TVG1-1-1	Py	5.82	IR05-TVG12-11	Py	5.83
20III-S4-TVG1-1-2	Py	5.60	IR05-TVG12-14	Py	6.57
20III-S4-TVG1-1-3	Py	5.47	IR05-TVG13-4-1	Cpy	7.54
20III-S4-TVG1-1-4	Py	5.20	IR05-TVG13-4-2	Sph	7.04
20III-S4-TVG1-2-1	Py	3.71	IR05-TVG13-9.1	Py	6.03
20III-S4-TVG1-2-2	Py	3.52	IR05-TVG13-9.1	Sulfate	21.5
20III-S4-TVG1-2-2	Cpy	3.82	IR05-TVG13-9.2-1	Sph	6.61
20III-S4-TVG1-2-3	Py	3.57	IR05-TVG13-9.2-2	Py	6.87
20III-S4-TVG1-2-3	Cpy	3.87	19III-S18-TVG9	Py	7.25
20III-S6-TVG3	Py	3.03	19III-S18-TVG9	Cpy	6.40
21III-S17-TVG13	Py	4.02	*LHF, MAR*		
13°N, EPR			MAR05-TVG1-9	Cpy	9.05
EPR05-TVG1-2-1	Py	2.21	MAR05-TVG1-10-3	Cpy	9.60
EPR05-TVG1-2-4	Py	2.05	MAR05-TVG1-21	Cpy	9.45
EPR05-TVG1-3-2	Py	1.91	*13°S, MAR*		
EPR05-TVG1-3-3	Py	1.53	21IV-S7-TVG4-1	Py	4.45
EPR05-TVG2-1-2	Py	1.43	*Area A, SWIR*		
EPR05-TVG2-1-4	Py	1.47	19II-S7-TVG4	Py	5.66
11°N, EPR			20V-S34-TVG16	Py	6.98
1384-2-2	Py	2.19	20V-S35-TVG17-1-1	Py	4.20
KHF, CIR			20V-S35-TVG17-3-2	Py	5.00
IR05-TVG-9-1	Py	1.82	20V-S35-TVG17-4-1	Py	4.40
IR05-TVG-9-2	Py	2.16	21VII-TVG22	Py	0.00
IR05-TVG-9-3	Py	2.25	*S99HF, NFB*		
25°S, CIR			26.1GTV-1	Sph	3.69
19III-S12-TVG6	Cpy	5.94	26.1GTV-2	Sph	4.07
EHF, CIR			26.2GTV-1	Sph	3.52
IR05-TVG12-5-2	Sph	6.38	26.2GTV-1	Py	2.73
IR05-TVG12-5-2	Py	5.22	26.2GTV-3	Sph	3.44
IR05-TVG12-8-2	Sph	6.14	42GTV-3	Py	3.84
IR05-TVG12-8-2	Py	6.25	113.1GTV-1	Cpy	4.21
IR05-TVG12-8-4	Py	6.30	113.1GTV-2	Py	2.80
IR05-TVG12-8-4	Sph	6.30	113.1GTV-4	Py	4.04
IR05-TVG12-9-1	Sph	6.30	113.1GTV-4	Cpy	3.97
IR05-TVG12-11	Sph	6.21	113.2GTV	Py	3.28

Py–pyrite; Cpy–chalcopyrite; Sph–sphalerite.

1992; Peter and Shanks, 1992; Lein et al., 1993; Zierenberg, 1994; Chiba et al., 1998; Gemmell and Sharpe, 1998; Herzig et al., 1998a, 1998b; Knott et al., 1998; Marumo and Hattori, 1999; Zeng et al., 2002a, 2002b; de Ronde et al., 2003; Kim et al., 2004; and Rouxel et al., 2004a). Sulfide minerals from the EPR near 1–2°S have much higher sulfur isotope ratios (pyrite $\delta^{34}S$ values from 3.0 to 5.8‰, avg. 4.4‰, n = 9; chalcopyrite $\delta^{34}S$ values from 3.8 to 3.9‰, n = 2) than in the EPR near 13°N and 11°N (pyrite $\delta^{34}S$ values from 1.4 to 2.2‰, avg. 1.9‰, n = 7) (Fig. 2A). These values are within the range of previously reported analyses of hydrothermal sulfides from the EPR near 13°N ($\delta^{34}S$ values from 0.4 to 5.0‰, avg. 2.7‰, n = 75, Bluth and Ohmoto, 1988; Stuart et al., 1995; Zeng et al., 2010), 11°N ($\delta^{34}S$ values from 2.2 to 4.9‰, avg. 4.1‰, n = 22, Bluth and Ohmoto, 1988; McConachy, 1988), and 21°N ($\delta^{34}S$ values from 0.7 to 6.2‰, avg. 2.5‰, n = 118, Hekinian et al., 1980; Arnold and Sheppard, 1981; Styrt et al., 1981; Kerridge et al., 1983; Zierenberg et al., 1984; Woodruff and Shanks, 1988; Stuart et al., 1994a) (see Table 3; Fig. 3).

In the MARs, the $\delta^{34}S$ value (4.5‰) of pyrite sample from the MAR near 13°S is significantly lower than that of chalcopyrite samples at the LHF ($\delta^{34}S$ values from 9.1 to 9.6‰) (Fig. 2B). These values are within the range of previously reported analyses of hydrothermal sulfides at the LHF (Bogdanov et al., 1997) (0.7 to 13.8‰, avg. 7.6‰, n = 26) but heavier than those of sulfides at the LHF reported by Petersen et al. (2005) (2.2 to 8.9‰, n = 21) and Rouxel et al. (2004b) (4.6 to 6.1‰, avg. 5.4‰, n = 17).

In the Indian Ocean, sulfide minerals at the EHF have much higher sulfur isotope ratios (pyrite $\delta^{34}S$ values from 5.2 to 7.3‰, avg. 6.3‰, n = 8; sphalerite $\delta^{34}S$ values from 6.1 to 7.0‰, avg. 6.4‰, n = 7; chalcopyrite $\delta^{34}S$ values from 6.4 to 7.5‰) than those in the KHF (pyrite $\delta^{34}S$ values from 1.8 to 2.3‰, avg. 2.1‰, n = 3), CIR near 25°S

(chalcopyrite $\delta^{34}S$ value 5.9‰, n = 1), and EPR near 13°N, 11°N, and 1–2°S (Fig. 2). The $\delta^{34}S$ values (0.0 to 7.0‰, avg. 4.4‰; n = 6) of sulfide minerals from the area A are lower than those of sulfides from the EHF (Table 2; Fig. 2), and the majority of these values are within the range of previously reported analyses of hydrothermal sulfides from the Sonne field in the CIR (from 1.6 to 6.6‰, avg. 3.4‰, n = 54, Halbach and Münch, 2000).

The $\delta^{34}S$ values in sulfide minerals at S99HF vary between 2.7 and 4.0‰ (avg. 3.3‰, n = 5) for pyrite, 3.4 and 4.1‰ (avg. 3.7‰, n = 4) for sphalerite, and 4.0 and 4.2‰ (avg. 4.1‰, n = 2) for chalcopyrite (Fig. 1D). These values are within the range of previously reported analyses of hydrothermal sulfides from the North Fiji basin (from 0.4 to 5.6‰, avg. 3.4‰, n = 78, Kim et al., 2006). Furthermore, compared to the sulfur isotopic compositions of sulfides from the sediment-hosted hydrothermal fields in the Middle Valley of the northern Juan de Fuca Ridge, the Escanaba Trough of the southern Gorda Ridge, and the Guaymas Basin of the Gulf of California, the sulfur isotopic compositions of sulfide minerals from the EPR near 13°N, 11°N, and 1–2°S, LHF, MAR near 13°S, KHF, EHF, CIR near 25°S, area A, and S99HF have a smaller range $\delta^{34}S$ values (see Table 3; Fig. 3).

In addition, if the pyrite and sphalerite had attained equilibrium at T = 150–250 °C, the differences (Δ) in the $\delta^{34}S$ values should be $\Delta_{pyrite-sphalerite}$ = 1.9–0.8‰, and pyrite should have a higher $\delta^{34}S$ than sphalerite (Smith et al., 1977). If the pyrite and chalcopyrite had attained equilibrium at T = 200–400 °C, the differences (Δ) in the $\delta^{34}S$ values should be $\Delta_{pyrite-chalcopyrite}$ = 2.0–1.0‰, and pyrite should have a higher $\delta^{34}S$ than chalcopyrite (Ohmoto and Rye, 1979). The pyrite–chalcopyrite pairs (sample 20III-S4-TVG1-2-2) from the EPR near 1–2°S, pyrite–sphalerite pairs (sample IR05-TVG12-5-2, IR05-TVG12-8-2, and IR05-TVG12-11) and sulfate–pyrite pairs (sample IR05-
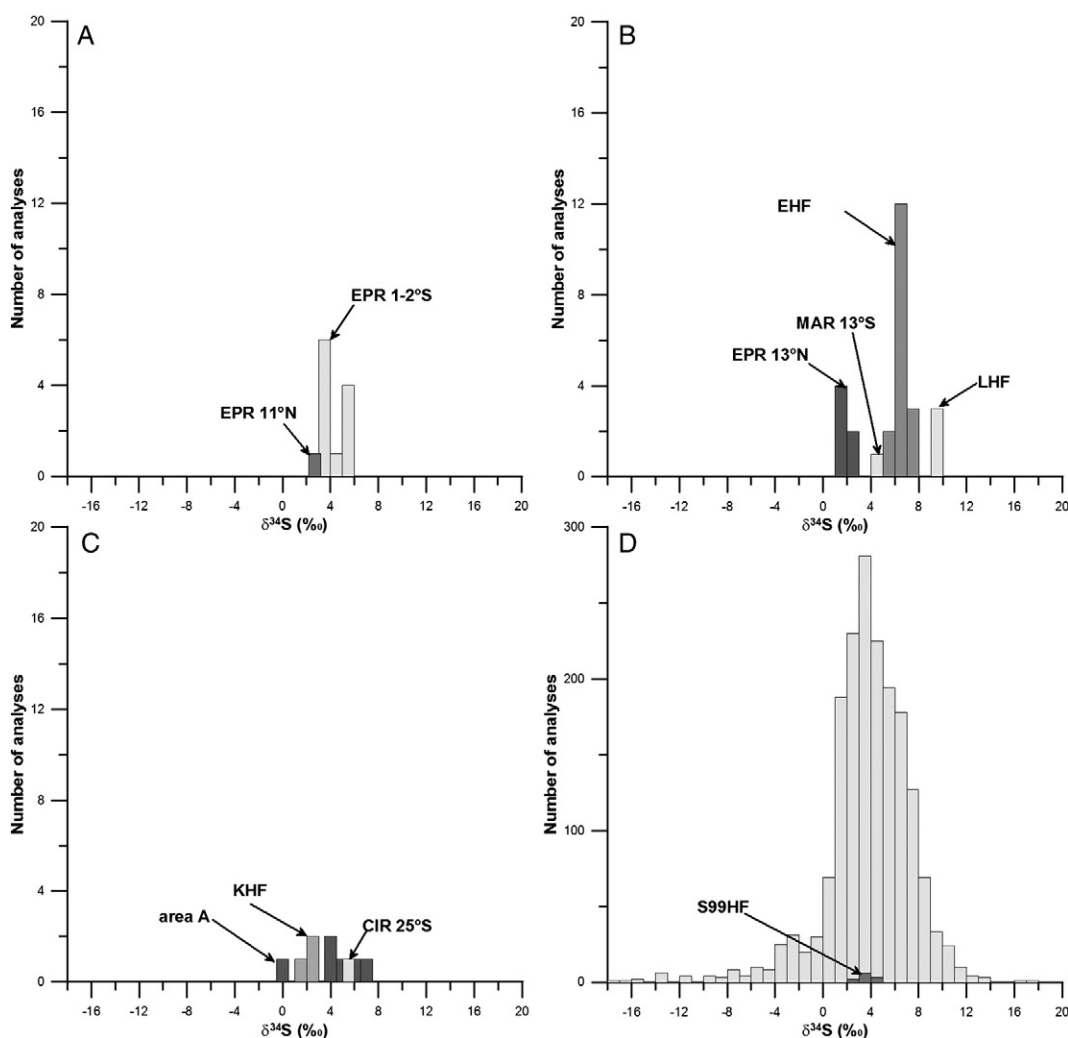
Fig. 2. Histogram of sulfur isotope values for sulfide samples from A: EPR near 1–2°S and 11°N; B: EPR near 13°N, LHF, EHF, and MAR near 13°S; C: KHF, CIR near 25°S, and area A; D: S99HF and other hydrothermal fields (including EPR near 21°S, 16°43′S, 7°24′S, 1–2°S, 9–10°N, 11°N, 13°N, and 21°N; Galapagos Rift; southern Juan de Fuca Ridge (SJdFR); Axial Seamount; Lucky Strike; Rainbow; Broken Spur; TAG; Snake Pit; LHF; MAR near 13°S; EHF; KHF; CIR near 25°S; area A on the SWIR; Middle Valley; Escanaba Trough; Guaymas Basin; Red Sea; Jade hydrothermal field; Mariana Trough; Manus Basin; NFB; Lau Basin; Myojinsho caldera; Conical Seamount; and Brothers Seamount). Sources of sulfur isotope data are in Table 2 and references are in Table 3.

TVG13-9.1) from the EHF, and the pyrite–sphalerite pairs (sample 26.2GTV-1) and pyrite–chalcopyrite pairs (sample 113.1GTV-4) from the S99HF exhibit sulfur isotopic disequilibrium, based on known temperature-dependent fractionation factors, typical of most seafloor hydrothermal systems (Ohmoto, 1986). Similar sulfur isotopic disequilibrium has been identified in most investigated seafloor hydrothermal sulfide deposits (e.g., the EPR at 21°N, Arnold and Sheppard, 1981; Styrt et al., 1981; Kerridge et al., 1983; Zierenberg et al., 1984; Woodruff and Shanks, 1988; the Guaymas Basin, Shanks and Niemitz, 1982; Koski et al., 1985 Peter and Shanks, 1992; the Red Sea, Shanks and Bischoff, 1977, 1980; the Axial Seamount, Hannington and Scott, 1988).

4.2. Lead isotopic compositions in sulfides

The Pb isotopic ratios of the sulfides from the EPR near 13°N, 11°N, and 1–2°S, LHF, MAR near 13°S, KHF, EHF, CIR near 25°S, area A, and S99HF range between 17.541 ± 0.004 and 19.268 ± 0.001 for $^{206}Pb/^{204}Pb$, 15.451 ± 0.001 and 15.684 ± 0.001 for $^{207}Pb/^{204}Pb$, 37.557 ± 0.008 and 38.988 ± 0.002 for $^{208}Pb/^{204}Pb$ ($n = 21$) (Table 4).

In the EPR near 13°N, the Pb isotopic composition of sulfides from the off-axis hydrothermal field in this study are more radiogenic than that of the hydrothermal sulfides from the older off-axis seamount and the marginal high of the EPR (Fouquet and Marcoux, 1995; Zeng

et al., 2010). The Pb isotopic composition of the three sulfide samples from the marginal high are closer to that of sulfide samples from the axial graben on the EPR near 13°N (Fouquet and Marcoux, 1995), with only one sample (EPR05-TVG1-3-1) possessing a more radiogenic Pb isotopic composition than sulfides from the axial graben. On the EPR near 1–2°S, three sulfide samples have similar Pb isotopic compositions, and the range of Pb isotopic compositions is narrow ($^{206}Pb/^{204}Pb = 18.156$ to 18.259; $^{207}Pb/^{204}Pb = 15.451$ to 15.512; $^{208}Pb/^{204}Pb = 37.635$ to 37.877) (Table 4), similar to that of sulfides from the EPR near 21°26′S (Fouquet and Marcoux, 1995) (see Table 5). Furthermore, the Pb isotopic composition of the three sulfide samples from the marginal high on the EPR near 13°N was more radiogenic than that of sulfides from the EPR near 1–2°S (see Table 5; Fig. 4). In the LHF, two samples (MAR05-TVG1-10-2 and MAR05-TVG1-9) show different Pb isotope compositions (Table 4; Fig. 5). The two sulfide samples have lower $^{206}Pb/^{204}Pb$ ratios (19.2 to 19.5) than that of sulfide samples from the Logatchev-1 hydrothermal field (Lein et al., 2001), but their $^{207}Pb/^{204}Pb$ ratios and $^{208}Pb/^{204}Pb$ ratios are similar to those of the Logatchev-1 hydrothermal field (Lein et al., 2001). In addition, the $^{207}Pb/^{204}Pb$ and $^{208}Pb/^{204}Pb$ ratios of one sulfide sample (MAR05-TVG1-9) from the LHF are within or near the range of pelagic sediments and Fe-Mn crusts from the Atlantic Ocean, respectively (Fig. 5), and the Pb isotopic composition of this sample is also similar to the Pb isotopic
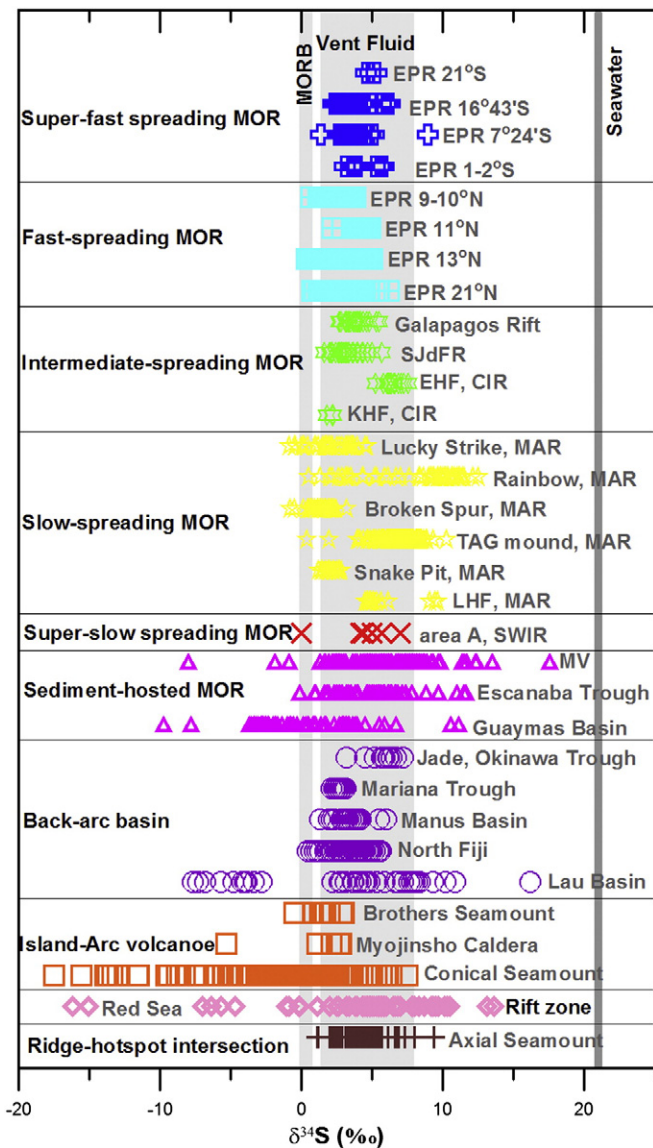
Fig. 3. Sulfur isotope values for sulfide samples from different hydrothermal fields (including EPR near 21°S, 16°43′S, 7°24′S, 1–2°S, 9–10°N, 11°N, 13°N, and 21°N; Galapagos Rift; SJdFR; EHF; KHF; Lucky Strike; Rainbow; Broken Spur; TAG; Snake Pit; LHF; area A; Middle Valley (MV); Escanaba Trough; Guaymas Basin; Jade; Mariana Trough; Manus Basin; North Fiji Basin; Lau Basin; Brothers Seamount; Myojinsho caldera; Conical Seamount; Red Sea; and Axial Seamount). Sources of sulfur isotope data are in Table 2 and references are in Table 3. MORB data are from Sakai et al. (1984), Alt et al. (1989), Shanks et al. (1995), and Alt and Shanks (2003). Vent fluid data are from Michard et al. (1984), Merlivat et al. (1987), Von Damm and Bischoff (1987), Campbell et al. (1988), Bluth and Ohmoto (1988), Bowers et al. (1988), Massoth et al. (1989), Butterfield et al. (1990), Shanks et al. (1995), and Shanks (2001). Seawater data is from Rees et al. (1978).

compositions of the sediment-hosted sulfide deposits currently forming at the sediment-filled Escanaba Trough of the Gorda Ridge (LeHuray et al., 1988; Zierenberg et al., 1993). Sulfide samples from the LHF have Pb isotope compositions that are significantly different from those of other sulfide samples from sediment-starved ridges (such as EPR 13°N, 21°N), which have particularly low $^{206}Pb/^{204}Pb$, $^{207}Pb/^{204}Pb$ and $^{208}Pb/^{204}Pb$ ratios (Table 5). In addition, one sulfide sample from the MAR near 13°S has significantly lower $^{206}Pb/^{204}Pb$, $^{207}Pb/^{204}Pb$, and $^{208}Pb/^{204}Pb$ ratios than sulfide samples from the LHF (Table 4; Fig. 5). The $^{206}Pb/^{204}Pb$ ratio is within the range of $^{206}Pb/^{204}Pb$ ratios of sulfide samples from the TAG hydrothermal field (Andrieu et al., 1998), but possesses a $^{207}Pb/^{204}Pb$ and $^{208}Pb/^{204}Pb$ ratios that are significantly higher (see Table 5). Sulfide samples from the KHF and CIR near 25°S has

significantly higher $^{206}Pb/^{204}Pb$, $^{207}Pb/^{204}Pb$ and $^{208}Pb/^{204}Pb$ ratios than basalts from the CIR near 25°S (Table 4; Fig. 6). The majority of Pb isotopic ratios in the four samples ($^{206}Pb/^{204}Pb$ = 17.898 to 17.984; $^{207}Pb/^{204}Pb$ = 15.453 to 15.562; $^{208}Pb/^{204}Pb$ = 37.815 to 38.173) from the EHF falls in the range of Pb isotopic composition fields of basalts from the CIR near 24°S (Table 4; Fig.6).

The range of Pb isotopic compositions of two sulfide samples in area A is narrow ($^{206}Pb/^{204}Pb$ = 18.149 to 18.208; $^{207}Pb/^{204}Pb$ = 15.484 to 15.491; $^{208}Pb/^{204}Pb$ = 37.988 to 37.997) (Table 4; Fig. 6). In comparison to sulfides from the EHF, they possess higher $^{206}Pb/^{204}Pb$ ratios, but similar $^{207}Pb/^{204}Pb$ and $^{208}Pb/^{204}Pb$ ratios (Table 4; Fig. 6). In the S99HF, the range of Pb isotopic compositions of four sulfide samples is narrow ($^{206}Pb/^{204}Pb$ = 18.139 to 18.160; $^{207}Pb/^{204}Pb$ = 15.493 to 15.514; $^{208}Pb/^{204}Pb$ = 37.960 to 38.001) (Table 4; Fig. 7), which is within the range of the Pb isotopic composition of sulfide samples (types 2 and 3 chimneys) from the North Fiji Basin (Kim et al., 2006). In addition, sulfides from the EPR near 13°N, the EPR near 1–2°S, the LHF, the MAR near 13°S, the EHF, the KHF, area A, and the S99HF possess Pb concentrations that span a large range (1.54 to 1905 ppm), and the Pb contents of three sulfide samples from the EHF are high (1312–1905 ppm), and are independent of the Pb isotope composition (Table 4).

5. Discussion

5.1. Sulfur sources

It is known that the hydrothermal activity on the EPR near 13°N, 11°N, and 1–2°S, MAR near 13°S, KHF, EHF, CIR near 25°S, area A, and S99HF are hosted by mid-ocean ridge basalts (MORBs). The sulfur in basalts uniformly have $\delta^{34}S$ values very close to 0‰ ($+0.1 \pm 0.5$‰) (Sakai et al., 1984; Alt et al., 1989; Shanks et al., 1995; Alt and Shanks, 2003). Furthermore, basaltic sulfur can be efficiently leached by high-temperature (300 °C–500 °C) fluid (Mottl et al., 1979), and large sulfur isotopic fractionation does not occur during leaching, transport, or reprecipitation as sulfide minerals (Shanks and Niemitz, 1982). Seawater sulfate has a $\delta^{34}S$ value of $+21$‰ (Rees et al., 1978). Hydrothermal vent fluids for seafloor sulfide–sulfate mineralization typically have $\delta^{34}S$ values of H_2S that range from 1.5‰ to 7‰ (e.g., Shanks et al., 1995), which fall between the $\delta^{34}S$ values for basalts ($+0.1 \pm 0.5$‰) and seawater ($+21$‰). Therefore, the sulfur isotopic compositions of seafloor sulfide deposits can be used as evidence for the source of sulfur (e.g., Fouquet et al., 1996).

The $\delta^{34}S$ values of sulfide mineral samples from the EPR near 13°N, 11°N, and 1–2°S, MAR near 13°S, KHF, EHF, CIR near 25°S, area A, and S99HF have a broad range (0.0 to 7.5‰; Table 2; Fig. 3), and are generally similar to the $\delta^{34}S$ values for hydrothermal vent fluids (1.5‰ to 7‰), which are between those of basalts and seawater (Table 2; Fig. 3).

On the MAR, the LHF is hosted by variable mixtures of serpentinized peridotite and mafic material (Delacour et al., 2008). The $\delta^{34}S$ values (9.1 to 9.6‰) of sulfide minerals at the LHF are higher than those of gabbros (-2.1 to 7.6‰; Delacour et al., 2008) from the southern wall of the Atlantis Massif. The $\delta^{34}S$ values of the sulfide minerals are also higher than those of oceanic gabbros and MORB (-2 to $+2$‰) (Sakai et al., 1984; Alt et al., 1989, 2007; Alt and Anderson, 1991). The sulfur isotopic compositions of the sulfide minerals at LHF indicate contributions of sulfur from both igneous rocks and seawater sulfate. Furthermore, the $\delta^{34}S$ values of sulfide minerals at the LHF are higher than basalt-hosted hydrothermal fields (e.g., EPR near 13°N, 11°N, and 1–2°S; Table 2), and are likely to have been influenced by reduction of seawater sulfate under higher fluid fluxes, more oxidizing conditions, and sulfide leaching from serpentinized peridotite and mafic material during high-temperature hydrothermal alteration (Alt et al., 2007; Delacour et al., 2008). In addition, the sulfur isotopic composition ($\delta^{34}S$ = 21.5‰) of the single sulfate sample at the EHF, which is indistinguishable from that of the seawater sulfate $\delta^{34}S$ value ($+21$‰; Rees et al., 1978), indicates that the sulfur in sulfate is derived from

Table 3

Comparison of sulfur isotopic compositions of seafloor hydrothermal sulfides from different deep-sea hydrothermal systems.

Field	δ^{34}S (‰)		Field	δ^{34}S (‰)	
	Range	Average (n)		Range	Average (n)
Super-fast spreading mid-ocean ridge			*Super-slow spreading mid-ocean ridge*		
21°S, EPR	+4.5–+5.3	+4.8 (4)	Area A, SWIR	0.0–+7.0	+4.4 (6)
16°43′S, EPR	+2.3–+6.3	+3.7 (49)	*Sediment-hosted mid-ocean ridge*		
7°24′S, EPR	+1.4–+8.9	+3.7 (31)	Middle Valley	−8.0–+12.4	+6.0 (190)
1–2°S, EPR	+3.0–+5.8	+4.3 (11)	Escanaba Trough	−0.1–+11.6	+5.0 (71)
Fast-spreading mid-ocean ridge			Guaymas Basin	−9.7–+11.1	−0.2 (92)
9–10°N, EPR	+0.7–+3.8	+2.6 (36)	*Back-arc basin*		
11°N, EPR	+2.2–+4.9	+4.1 (22)	Jade, Okinawa Trough	+3.2–+7.2	+5.9 (14)
13°N, EPR	+0.4–+5.0	+2.7 (75)	Mariana Trough	+2.1–+3.1	+2.7 (18)
21°N, EPR	+0.7–+6.2	+2.5 (118)	Manus Basin	−8.0–+6.0	+1.2 (54)
Intermediate-spreading mid-ocean ridge			North Fiji Basin	+0.4–+5.6	+3.5 (89)
Galapagos 86°W	+2.8–+5.5	+3.9 (21)	Vai Lili, Lau Basin	+7.2–+16.2	+9.4 (13)
SJdFR	+1.6–+5.7	+3.2 (44)	White Church, Lau Basin	+2.2–+6.8	+4.2 (20)
EHF, CIR	+5.2–+7.5	+6.4 (17)	Hine Hina, Lau Basin	−7.2 to −2.8	−5.0 (12)
KHF, CIR	+1.8–+2.3	+2.1 (3)	*Island-Arc volcano*		
Slow-spreading mid-ocean ridge			Myojinsho Caldera	−5.3–+2.8	+1.0 (6)
Lucky Strike, MAR	−0.9–+4.6	+2.4 (65)	Conical Seamount	−17.5–+6.1	−1.9 (129)
Rainbow, MAR	+0.5–+12.5	+8.0 (64)	Brothers Seamount	−0.5–+2.9	+1.6 (8)
Broken Spur, MAR	−0.8–+3.2	+1.3 (48)	*Rift zone*		
TAG, MAR	+0.35–+10.27	+6.7 (287)	Red Sea	−16.2–+23.4	+4.9 (74)
Snakepit, MAR	+1.2–+2.8	+2.1 (16)	*Ridge-hotspot intersection*		
LHF, MAR	+4.5–+9.6	+5.7 (20)	Axial seamount, JdFR	+1.1–+9.4	+4.2 (113)

Data are from: 21°S, EPR (Ono et al., 2007); 16°43′S, EPR (Marchig et al., 1997); 7°24′S, EPR (Marchig et al., 1997); 1–2°S, EPR (this study, see Table 2); 9–10°N, EPR (Ono et al., 2007; Rouxel et al., 2008); 11°N, EPR (Bluth and Ohmoto, 1988); 13°N, EPR (Bluth and Ohmoto, 1988; Ono et al., 2007; Stuart et al., 1995; Zeng et al., 2010; partly data from this study, see Table 2); 21°N, EPR (Arnold and Sheppard, 1981; Hekinian et al., 1980; Kerridge et al., 1983; Stuart et al., 1994a; Woodruff and Shanks, 1988; Zierenberg et al., 1984); Galapagos 86°W (Knott et al., 1995); SJdFR (Shanks and Seyfried, 1987); Edmond, CIR (this study, see Table 2); Kairei, CIR (this study, see Table 2); Lucky Strike, MAR (Ono et al., 2007; Rouxel et al., 2004a; Rouxel et al., 2004b); Rainbow, MAR (Lein et al., 2001; Rouxel et al., 2004b); Broken Spur, MAR (Butler et al., 1998; Duckworth et al., 1995); TAG, MAR (Chiba et al., 1998; Gemmell and Sharpe, 1998; Herzig et al., 1998a; Knott et al., 1998; Lein et al., 1991; Stuart et al., 1994a; Zeng et al., 2000a); Snakepit, MAR (Kase et al., 1990; Stuart et al., 1994a); Logatchev, MAR (Rouxel et al., 2004b; partly data from this study, see Table 2); A area, SWIR (this study, see Table 2); Middle Valley (Duckworth et al., 1994; Goodfellow and Franklin, 1993; Stuart et al., 1994a, 1994b; Zierenberg, 1994); Escanaba Trough (Böhlke and Shanks, 1994; Koski et al., 1988; Zierenberg et al., 1993; Zierenberg and Shanks, 1994); Guaymas Basin (Koski et al., 1985; Peter and Shanks, 1992; Shanks and Niemitz, 1982); Jade, Okinawa Trough (Halbach et al., 1989; Marumo and Hattori, 1999; Zeng et al., 2002a); Mariana Trough (Kusakabe et al., 1990); Manus Basin (Lein et al., 1993; Kim et al., 2004); North Fiji Basin (Kim et al., 2006; partly data from this study, see Table 2); Lau Basin (Herzig et al., 1998b); Myojinsho Caldera (Iizasa et al., 1992); Conical Seamount (Gemmell et al., 2004; Petersen et al., 2002); Brothers Seamount (de Ronde et al., 2003); Red Sea (Blum and Puchelt, 1991; Zierenberg and Shanks, 1988); Axial seamount, JdFR (Crowe and Valley, 1992; Hannington and Scott, 1988). JdFR-Juan de Fuca Ridge; SJdFR-Southern Juan de Fuca Ridge. n - number of samples.

seawater, which can be interpreted as evidence of entrainment of seawater into hydrothermal fluids within the chimney.

Furthermore, according to a simple two end-member mixing model ($\delta^{34}S_{mix} = X \times \delta^{34}S_{seawater} + (1 - X) \times \delta^{34}S_{basalt}$; where X is the amounts of seawater component; $\delta^{34}S_{mix}$, $\delta^{34}S_{seawater}$ (21‰), and $\delta^{34}S_{basalt}$ (0‰) are the sulfur isotopic compositions of sulfide, seawater, and basalt, respectively), the sulfur isotopic composition of sulfide minerals can be explained by disequilibrium mixing of sulfur (about 6–10%, 10%, 14–27%, 21%, 8–11%, 28%, 25–36%, 0–33%, and 12–20%) from reduced seawater sulfate with sulfur (about 90–94%, 90%, 73–86%, 79%, 89–92%, 72%, 64–75%, 67–100%, and 80–88%) of basaltic origin in the EPR near 13°N, 11°N, and 1–2°S, MAR near 13°S, KHF, EHF, CIR near 25°S, area A, and S99HF, suggesting that the contribution proportions of seawater sulfur are lower than that of basaltic sulfur in the hydrothermal sulfide minerals from the EPR near 13°N, 11°N, and 1–2°S, MAR near 13°S, KHF, EHF, CIR near 25°S, area A, and S99HF.

5.2. Lead sources

The majority of Pb isotope ratios of sulfides from the EPR near 13°N and 1–2°S, MAR near 13°S, EHF, CIR near 25°S, area A, and S99HF fall in the range of Pb isotopic composition fields of basalts from the EPR, MAR, Indian ridge (IR) and North Fiji Basin (Figs. 4–7), suggesting that basalts are the principal source of lead for hydrothermal fluids (e.g., Vidal and Clauer, 1981; Chen, 1987; Hegner and Tatsumoto, 1987; Hinkley and Tatsumoto, 1987; Fouquet and Marcoux, 1995; Charlou et al., 2002; Yao et al., 2009). Furthermore, the Pb isotope data of seafloor hydrothermal sulfides define a small domain compared with the larger field of mid-ocean ridge and back-arc basin basalts. The mean Pb isotopic compositions of sulfides from the EHF, CIR near 25°S, area A, and S99HF (Table 5) are similar to that of basalts from the vicinity of the

respective hydrothermal field, which suggests that the heterogeneous Pb isotope (e.g., Allègre et al., 1984; Hamelin et al., 1984) extracted from the upper oceanic crust by hydrothermal fluid are homogenized during hydrothermal circulation, supporting the conclusion of previous studies (Fouquet and Marcoux, 1995; Andrieu et al., 1998). In turn, this suggests that the average Pb isotopic composition of sulfide minerals can be used to infer the Pb isotopic composition of the local basaltic crust.

The Pb isotopic ratios of sulfides from the EPR near 13°N and 1–2°S and CIR near 25°S appear to be close to the average values of Pb isotope ratios of basalts in the EPR near 13°N and 1–2°S, and CIR near 25°S, respectively (Figs. 4 and 6), implying that seawater is not a possible source of the Pb in the sulfides. Furthermore, in the KHF, one sulfide sample (IR05-TVG-9-2) also has higher ^{207}Pb/^{204}Pb and ^{208}Pb/^{204}Pb ratios (i.e., is more radiogenic) than sulfides from the EHF and the CIR near 25°S. The Pb isotope composition plots near or within those of the Indian Ridge basaltic field, suggesting that seawater could not be a component of the source of Pb in the KHF (Fig. 6). In addition, the more radiogenic Pb isotope composition of sulfide samples from the S99HF compared to that of type 1 chimneys (^{206}Pb/^{204}Pb = 18.082 to 18.132; ^{207}Pb/^{204}Pb = 15.440 to 15.481; ^{208}Pb/^{204}Pb = 37.764 to 37.916) from the 16°53′S triple junction area in the North Fiji Basin, suggest that the Pb in the sulfides is possibly related to E-MORB volcanism, which shows higher Pb isotope ratios than do N-MORB rocks (Kim et al., 2006).

5.3. Variable sulfur isotopic compositions

The δ^{34}S values of sulfide samples from the EPR near 13°N, 11°N, and 1–2°S, LHF, MAR near 13°S, KHF, EHF, CIR near 25°S, area A, and S99HF vary from 0.0 to 9.6‰. The variation in the sulfur isotope compositions of sulfides from different hydrothermal systems is related to the sulfate

Table 4
Lead isotopic compositions of seafloor massive sulfide samples from EPR near 1–2°S and 13°N, KHF, CIR near 25°S, EHF, LHF, MAR near 13°S, area A, and S99HF.

Sample no.	Mineralogy	$^{206}Pb/^{204}Pb$	$^{207}Pb/^{204}Pb$	$^{208}Pb/^{204}Pb$	Pb (ppm)
1–2°S, EPR					
20III-S4-TVG1-1-2	Py	18.185 ± 0.001	15.488 ± 0.001	37.760 ± 0.002	78.8
20III-S4-TVG1-2-3	Cpy + Py ± Sph	18.156 ± 0.001	15.451 ± 0.001	37.635 ± 0.003	77.9
20III-S6-TVG3	Py + Sph	18.259 ± 0.002	15.512 ± 0.002	37.877 ± 0.005	560
13°N, EPR					
EPR05-TVG1-2-2	Py	18.431 ± 0.001	15.518 ± 0.001	37.974 ± 0.002	59.3
EPR05-TVG1-3-1	Py	18.457 ± 0.001	15.553 ± 0.001	38.080 ± 0.002	99.7
EPR05-TVG2-1-1	Py + Sph ± Cpy	18.419 ± 0.001	15.506 ± 0.001	37.920 ± 0.004	256
KHF, CIR					
IR05-TVG-9-2	Py	18.471 ± 0.002	15.597 ± 0.002	38.406 ± 0.007	37.3
25°S, CIR					
19III-S12-TVG6	Cpy ± CuS ± oxide	17.553 ± 0.004	15.503 ± 0.004	37.600 ± 0.010	1.54
19III-S12-TVG6[a]	Cpy ± CuS ± oxide	17.541 ± 0.004	15.491 ± 0.003	37.557 ± 0.008	
EHF, CIR					
IR05-TVG12-14	Py	17.898 ± 0.001	15.453 ± 0.001	37.815 ± 0.002	1905
IR05-TVG13-4-2	Cpy + Py	17.957 ± 0.001	15.515 ± 0.001	38.023 ± 0.005	1374
IR05-TVG13-9.2-1	Py + Sph + Cpy	17.984 ± 0.002	15.562 ± 0.002	38.173 ± 0.007	1312
19III-S18-TVG9	Py ± sulfate	17.921 ± 0.001	15.483 ± 0.001	37.910 ± 0.003	442
LHF, MAR					
MAR05-TVG1-9	Cpy + CuS + Py ± sulfate (<1%)	18.698 ± 0.001	15.684 ± 0.001	38.988 ± 0.002	19.1
MAR05-TVG1-10-2	Py + Cpy ± sulfate (2%)	19.268 ± 0.001	15.583 ± 0.001	38.959 ± 0.002	15.4
13°S, MAR					
21IV-S7-TVG4-1	Py	18.310 ± 0.002	15.534 ± 0.002	38.172 ± 0.007	850
Area A, SWIR					
20V-S35-TVG17-7	Py	18.208 ± 0.001	15.491 ± 0.001	37.997 ± 0.002	–
21VII-TVG22	Py	18.149 ± 0.002	15.484 ± 0.002	37.988 ± 0.005	17.4
S99HF, NFB					
26.2GTV-2	Py + Sph	18.146 ± 0.001	15.514 ± 0.001	38.001 ± 0.003	1198
42GTV-2	Py + Cpy	18.160 ± 0.001	15.493 ± 0.001	37.969 ± 0.003	965
113.1GTV-3	Py + Cpy	18.146 ± 0.001	15.505 ± 0.001	37.983 ± 0.002	781.6
113.2GTV	Py	18.139 ± 0.001	15.499 ± 0.001	37.960 ± 0.002	1343

All Pb isotopic ratios measured by static mode were corrected for instrumental mass fractionation through repeated analyses of the NBS 981 standard. Analytical error (2σ) is reported for each ratio. The Pb contents of the hydrothermal sulfide samples were determined on separate 40 mg splits of bulk sulfide by ICP-AES, relative standard deviation (RSD) <2%. [a] indicates the repeated analysis sample; "–" indicates no data available.

reduction, the residence time of fluids, and the multiple-stages of hydrothermal activity (e.g., Shanks and Seyfried, 1987; Bluth and Ohmoto, 1988; Peter and Shanks, 1992; Knott et al., 1995, 1998). Sulfate reduction is favored during slow seawater–fluid mixing in the chimney walls or within a mound, with isotopic fractionation approaching equilibrium values, and ^{34}S-enriched sulfide is produced by the reduction of seawater sulfate during subsurface reaction with ferrous iron-bearing minerals (Peter and Shanks, 1992), implying that the sulfate reduction homogenizes the sulfur isotopic composition of sulfides. Furthermore, the longer residence time of fluids in a hydrothermal system such as TAG might lead to more extensive local sulfate reduction (Knott et al., 1998). Therefore, the change in the $\delta^{34}S$ values of sulfide samples from the EPR near 1–2°S (3.0 to 5.8‰, see Table 2), and area A (0.0 to 7.0‰, see Table 2) is attributed to the increased contribution of H_2S derived from reduction of seawater sulfate in the subsurface hydrothermal zone, compared to the H_2S solely leached from the host basalt in deeper parts of the hydrothermal system. In addition, the variations in the $\delta^{34}S$ values of the sulfides were probably caused by rapid chemical reactions of dissolution, reprecipitation, and replacement (e.g., anhydrite is replaced by sulfide with high $\delta^{34}S$ values inherited for the seawater) between hydrothermal fluids and earlier sulfide and sulfate minerals in the hydrothermal sulfide deposits, rather than by kinetic isotope effects during precipitation of hydrothermal sulfides (Shanks and Seyfried, 1987; Bluth and Ohmoto, 1988). Furthermore, in the EPR near 13°N, LHF, EHF, KHF, and S99HF, the $\delta^{34}S$ values of pyrite, chalcopyrite, and sphalerite minerals are strikingly similar (Table 2), indicating a constant sulfur source and a very similar precipitation mechanism (Shanks and Bischoff, 1980). The similarities suggest that the pyrite, chalcopyrite,

and sphalerite minerals are formed by a single-stage hydrothermal fluid. The sulfur source and sulfide producing reactions must have been very similar during the single-stage hydrothermal mineralization.

In addition, the variations in the sulfur isotopic compositions of sulfides or sulfate can be studied by using the discrete degree and variation rate:

$$\delta^{34}S \text{ discrete degree } (\%) = \left[\sum \left(\delta^{34}S_i - \delta^{34}S_{ave}\right)/(n-1)\right]^{0.5}/\delta^{34}S_{ave} \quad (1)$$

where i = 1, 2, 3, n; n is the sample number; and $\delta^{34}S_{ave} = \sum (\delta^{34}S)_i / n$;

$$\delta^{34}S \text{ variation rate } (\%) = \left(\delta^{34}S_{max} - \delta^{34}S_{min}\right)/\delta^{34}S_{ave} \quad (2)$$

where $\delta^{34}S_{max}$ is the maximum value of sulfur isotope compositions in sulfide or sulfate samples from the same hydrothermal field, $\delta^{34}S_{min}$ is the minimum value of sulfur isotope compositions in sulfide or sulfate samples from the same hydrothermal field, and $\delta^{34}S_{ave}$ is the average value of sulfur isotope ratios in sulfide or sulfate samples from the same hydrothermal field.

The discrete degree and variation rate in the sulfur isotope compositions of sulfides from the super-slow, and slow spreading (full spreading rate < 50 mm/yr) MORs are larger than those from the super-fast and fast spreading (full spreading rate > 80 mm/yr) MORs (Fig. 8). Further, the ranges of sulfur isotopic compositions of sulfides in the super-slow ($\delta^{34}S$ values 0.0 to 7.0‰, area A), and slow ($\delta^{34}S$ values 4.5 to 9.6‰, LHF) spreading MORs are larger than those in the super-fast ($\delta^{34}S$ values

Table 5
Comparison of Pb isotope compositions of seafloor massive sulfides from different deep-sea hydrothermal systems.

Field	$^{206}Pb/^{204}Pb$		$^{207}Pb/^{204}Pb$		$^{208}Pb/^{204}Pb$	
	Range	Average (n)	Range	Average (n)	Range	Average (n)
Super-slow spreading mid-ocean ridge						
Area A, SWIR	18.149–18.208	18.178 (2)	15.484–15.491	15.488 (2)	37.988–37.997	37.992 (2)
Slow-spreading mid-ocean ridge						
TAG, MAR	18.202–18.365	18.266 (51)	15.408–15.522	15.477 (51)	37.583–37.938	37.794 (51)
LHF, MAR	18.698–19.268	18.983 (2)	15.583–15.684	15.633 (2)	38.959–38.988	38.974 (2)
Intermediate-spreading mid-ocean ridge						
25°S, CIR	17.541–17.553	17.547 (2)	15.491–15.503	15.497 (2)	37.557–37.600	37.579 (2)
EHF, CIR	17.898–17.984	17.940 (4)	15.453–15.562	15.503 (4)	37.815–38.173	37.980 (4)
Galapagos 86°W	18.563–18.603	18.582 (3)	15.501–15.561	15.531 (3)	38.085–38.250	38.159 (3)
Explorer Ridge	18.587–19.041	18.875 (3)	15.456–15.549	15.509 (3)	37.996–38.326	38.189 (3)
Endeavour Segment	18.678–18.769	18.722 (18)	15.467–15.566	15.510 (18)	37.957–38.276	38.092 (18)
SJdFR	18.444–18.466	18.457 (10)	15.447–15.468	15.458 (10)	37.728–37.838	37.784 (10)
Fast-spreading mid-ocean ridge						
21°N, EPR	18.441–18.494	18.470 (18)	15.464–15.508	15.492 (18)	37.810–37.983	37.898 (18)
13°N, EPR	18.341–18.457	18.400 (32)	15.462–15.553	15.502 (32)	37.800–38.080	37.900 (32)
Super-fast spreading mid-ocean ridge						
1–2°S, EPR	18.156–18.259	18.200 (3)	15.451–15.512	15.484 (3)	37.635–37.877	37.757 (3)
17°26′S, EPR	18.698–18.707	18.703 (2)	15.532–15.544	15.538 (2)	38.265–38.277	38.271 (2)
18°31′S, EPR	18.538–18.580	18.561 (3)	15.491–15.514	15.504 (3)	37.980–38.095	38.055 (3)
21°26′S, EPR	18.220–18.257	18.232 (5)	15.463–15.501	15.476 (5)	37.647–37.768	37.704 (5)
Sediment-hosted mid-ocean ridge						
Middle Valley	17.350–18.910	18.799 (75)	15.470–15.670	15.580 (75)	37.220–38.770	38.438 (75)
Escanaba Trough	18.899–19.152	19.062 (9)	15.624–15.689	15.654 (9)	38.794–39.237	39.069 (9)
Guaymas Basin	18.757–18.799	18.778 (2)	15.583–15.617	15.600 (2)	38.412–38.559	38.486 (2)
Back-arc basin						
Jade, Okinawa Trough	18.491–18.609	18.544 (13)	15.580–15.684	15.622 (13)	38.570–38.859	38.696 (13)
Eastern Manus Basin	18.760–18.780	18.775 (6)	15.520–15.540	15.530 (6)	38.310–38.400	38.357 (6)
North Fiji Basin	18.082–18.193	18.138 (19)	15.440–15.554	15.492 (19)	37.764–38.150	37.949 (19)
Lau Basin	18.615–18.690	18.667 (4)	15.531–15.550	15.540 (4)	38.287–38.327	38.310 (4)
Off-axis volcanoes						
Pito Seamount	18.448–18.520	18.493 (6)	15.482–15.583	15.548 (6)	37.784–38.208	38.035 (6)
Ridge-hotspot intersections						
Axial seamount, JdFR	18.598–18.613	18.608 (3)	15.457–15.458	15.457 (3)	37.994–38.109	38.041 (3)

Data are from: area A, SWIR (this study, see Table 4); TAG, MAR (Andrieu et al., 1998; Zeng et al., 2000b); LHF, MAR (this study, see Table 4); 25°S, CIR (this study, see Table 4); EHF, CIR (this study, see Table 4); Galapagos 86°W (Fouquet and Marcoux, 1995; LeHuray et al., 1988); Explorer Ridge (Fouquet and Marcoux, 1995); Endeavour Segment (LeHuray et al., 1988; Yao et al., 2009); SJdFR (LeHuray et al., 1988; Hegner and Tatsumoto, 1987); 21°N, EPR (Brévart et al., 1981; Vidal and Clauer, 1981); 13°N, EPR (Fouquet and Marcoux, 1995; Zeng et al., 2010; this study, see Table 4); 1–2°S, EPR (this study, see Table 4); 17°26′S, EPR (Fouquet and Marcoux, 1995); 18°31′S, EPR (Fouquet and Marcoux, 1995); 21°26′S, EPR (Fouquet and Marcoux, 1995); Middle Valley (Bjerkgård et al., 2000; Stuart et al., 1999; Cousens et al., 2002; Goodfellow and Franklin, 1993; Fouquet and Marcoux, 1995); Escanaba Trough (Zierenberg et al., 1993; LeHuray et al., 1988); Guaymas Basin (LeHuray et al., 1988); Jade, Okinawa Trough (Halbach et al., 1997; Zeng et al., 2000a); Eastern Manus Basin (Kim et al., 2004); North Fiji Basin (Kim et al., 2006; this study, see Table 4); Lau Basin (Fouquet and Marcoux, 1995); Pito Seamount (Verati et al., 1999); Axial seamount, JdFR (LeHuray et al., 1988). JdFR- Juan de Fuca Ridge; SJdFR-Southern Juan de Fuca Ridge. n - number of samples.

3.0 to 5.8‰, EPR near 1–2°S) and fast ($\delta^{34}S$ values 0.4 to 5.0‰, EPR near 13°N) spreading MORs (Fig. 9, Table 3).

The large variation in the sulfur isotopic composition of the sulfides in the super-slow, and slow spreading MORs can be explained by the multi-sulfur sources (seawater, basalt, serpentinized peridotite, mafic material, magmatic degassing, sediment) of sulfides (such as in the Guaymas Basin and the Middle Valley in sediment-hosted, slow-spreading MORs, Lau basin) (Shanks and Niemitz, 1982; Koski et al., 1988; Peter and Shanks, 1992; Zierenberg et al., 1993; Duckworth et al., 1994; Zierenberg, 1994; Herzig et al., 1998a). In addition, the degree of fluid–basalt interaction, and/or fluid–seawater mixing are recorded in sulfides as a gradual shift to decreasing (close to 0‰), or increasing (close to 21‰) $\delta^{34}S$ values, respectively (Fig. 10). The larger (>50%) or smaller (<50%) basalt/seawater sulfur ratios indicate that the majority of sulfur in the sulfide samples is from basalt or seawater, respectively. In the super-fast and fast spreading MORs, the majority of basalt/seawater sulfur ratios in the sulfides are from 70 to 100%, suggesting that the sulfur isotope compositions of sulfides are controlled by the degree of fluid–basalt interaction and fluid–seawater mixing (Fig. 10). In the super-slow, slow, and intermediate spreading ridges, the variation of basalt/seawater sulfur ratios in sulfides range from 40 to >100% (Fig.

10). The larger basalt/seawater sulfur ratios (>100%) in sulfides can result from the magmatic degassing and/or bacterial activity (Fig. 10), as the magmatic degassing and/or bacterial activity can cause the $\delta^{34}S$ values of sulfides to be lower than 0‰, for example, sulfides in the Hine Hina hydrothermal field (full spreading rate 60 mm/yr) of Lau Basin (Herzig et al., 1998a) and the Guaymas Basin hydrothermal systems (full spreading rate 45 mm/yr) (Peter and Shanks, 1992).

5.4. Variable lead isotopic compositions

The variability of basaltic Pb isotope composition along the mid-ocean ridges is a major cause of Pb isotopic variations in associated seafloor hydrothermal sulfides (Church and Tatsumoto, 1975; Tatsumoto, 1978; Sun, 1980; Vidal and Clauer, 1981; Hamelin et al., 1984). At the EPR near 13°N and 1–2°S, the EHF, the CIR near 25°S, and the S99HF, the range of Pb-isotope compositions in the sulfides is much smaller than in basalts (Figs. 4–7), and the Pb isotopic ratios of sulfides show only minor variations (Table 4), suggesting a common source for the Pb of all sulfides from the EPR near 13°N, the EPR near 1–2°S, the EHF, the area A, and the S99HF.
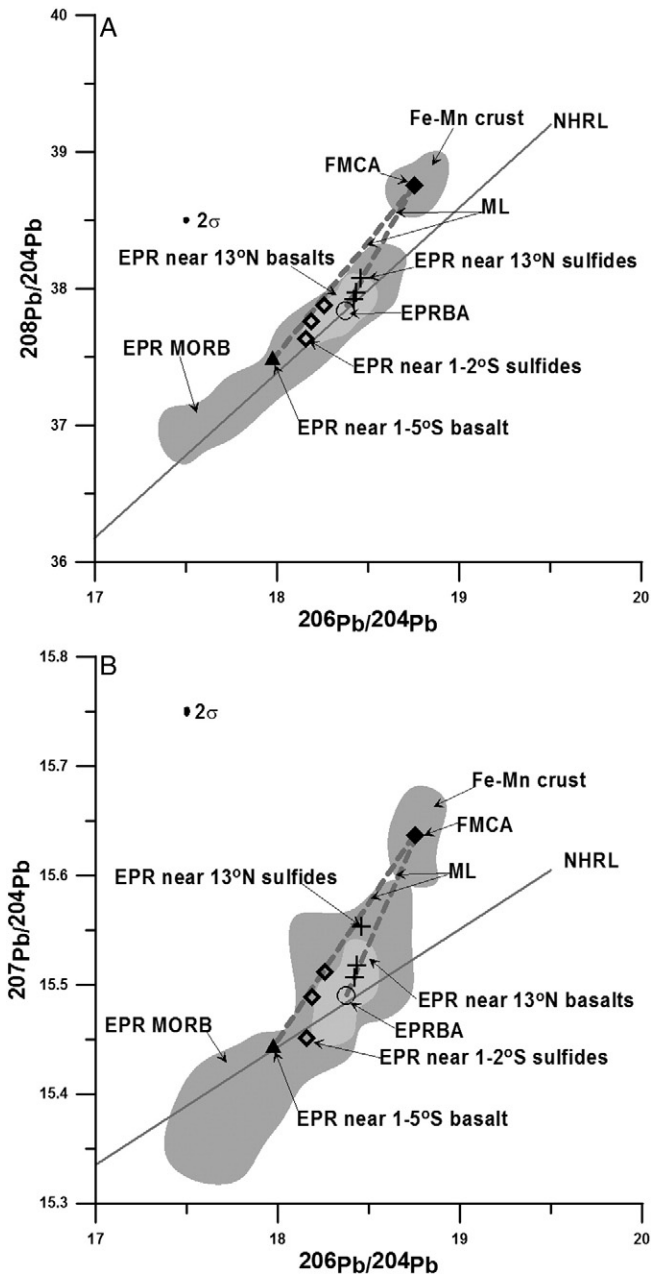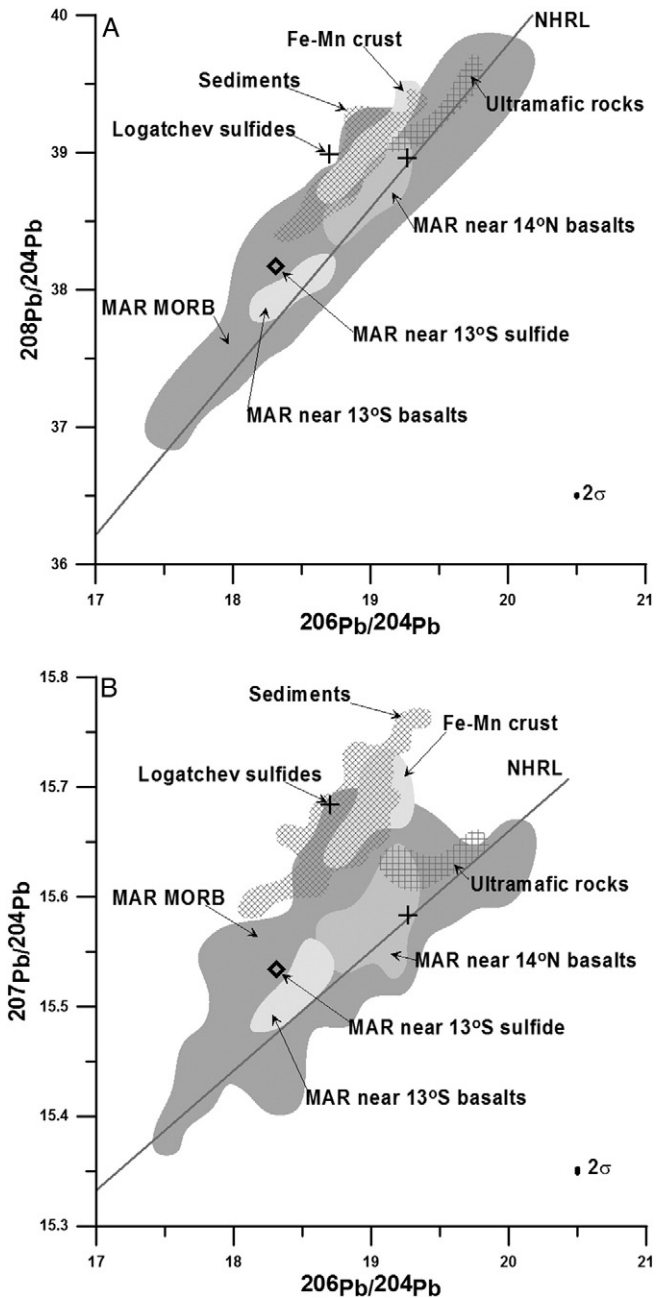
Fig. 4. A: $^{208}Pb/^{204}Pb$ vs. $^{206}Pb/^{204}Pb$; B: $^{207}Pb/^{204}Pb$ vs. $^{206}Pb/^{204}Pb$ plots for hydrothermal sulfides from EPR near 13°N and 1–2°S. EPR near 13°N basalts, EPR near 1–5°S basalt, and EPR MORB are from the updated PetDB database (http://www.petdb.org). Fe-Mn crust data are from Von Blanckenburg et al. (1996). FMCA is average value of the Pb isotope ratios in Fe-Mn crust. EPRBA is average value of the Pb isotope ratios in EPR near 13°N basalts. ML is mixing line between Pb isotope compositions of FMCA and EPRBA, and mixing line between Pb isotope compositions of FMCA and EPR near 1–5°S basalt. NHRL is Northern Hemisphere Reference Line (Hart, 1984). Maximum 2σ error for all sulfide samples is also plotted.

The variations in the Pb isotopic compositions of sulfides can also be studied by using the discrete degree and variation rate:

$$Pb\ discrete\ degree\ (\%) = \left\{ \sum \left[(Pb)_i - (Pb)_{ave} \right] / (n-1) \right\}^{0.5} / (Pb)_{ave} \quad (3)$$

where $Pb = {}^{206}Pb/^{204}Pb$, $^{207}Pb/^{204}Pb$, and $^{208}Pb/^{204}Pb$; $I = 1, 2, 3, n$; n is the sample number; $(Pb)_{ave.} = \sum (Pb)_i/n$.

$$Pb\ variation\ rate\ (\%) = (Pb_{max} - Pb_{min}) / Pb_{ave} \quad (4)$$

Fig. 5. A: $^{208}Pb/^{204}Pb$ vs. $^{206}Pb/^{204}Pb$; B: $^{207}Pb/^{204}Pb$ vs. $^{206}Pb/^{204}Pb$ plots for hydrothermal sulfides from Logatchev hydrothermal field and MAR near 13°S. Ultramafic rocks, MAR near 14°N basalts, MAR near 13°S basalt, and MAR MORB are from the updated PetDB database (http://www.petdb.org). Fe-Mn crust data are from Von Blanckenburg et al. (1996). Sediments data are from Ben Othman et al. (1989). NHRL is Northern Hemisphere Reference Line (Hart, 1984). Maximum 2σ error for all sulfide samples is also plotted.

where Pb_{max} is the maximum ratio of Pb isotope compositions in the sulfide samples from the same hydrothermal field, Pb_{min} is the minimum ratio of Pb isotope compositions in the sulfide samples from the same hydrothermal field, and Pb_{ave} is the average value of Pb isotope ratios in sulfide samples from the same hydrothermal field.
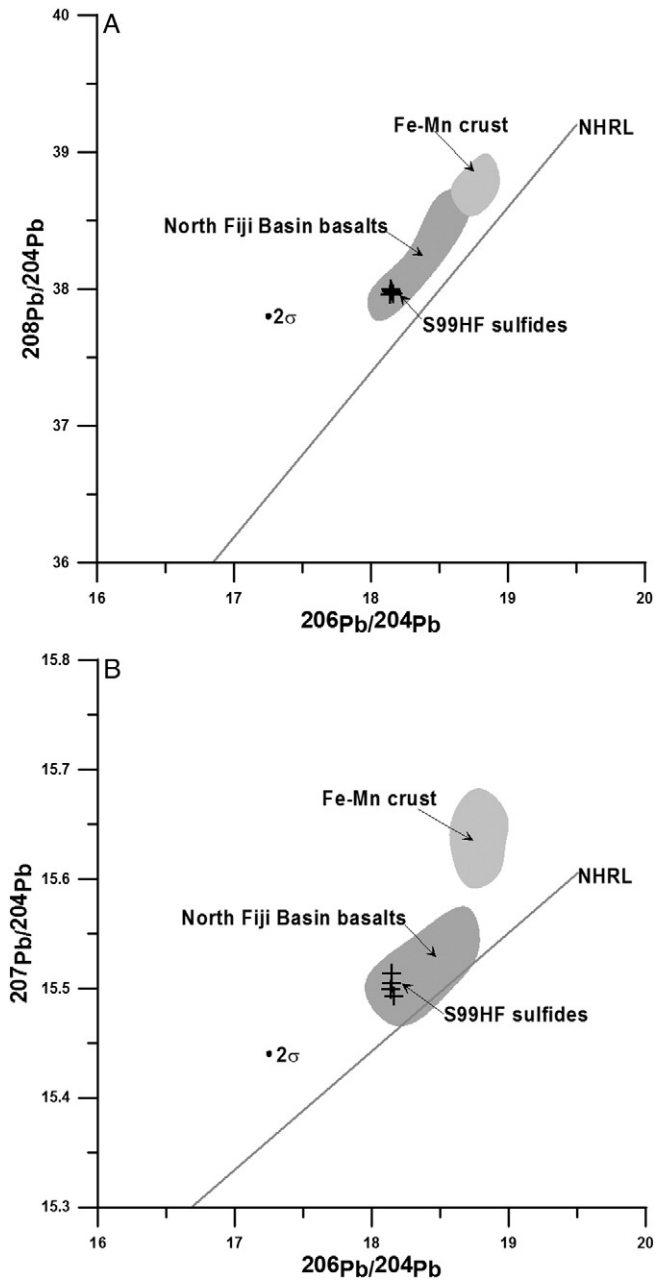
There is no clear relationship between the variation rate in the Pb isotope compositions of sulfides from different ridge segments and the local spreading rate of the mid-ocean ridge, suggesting that the spreading rate of a mid-ocean ridge does not significantly affect the Pb isotopic compositions in the sulfides from a local hydrothermal field.

The variation in the Pb isotope compositions of sulfides from different hydrothermal systems is related to the Pb sources of sulfides and the
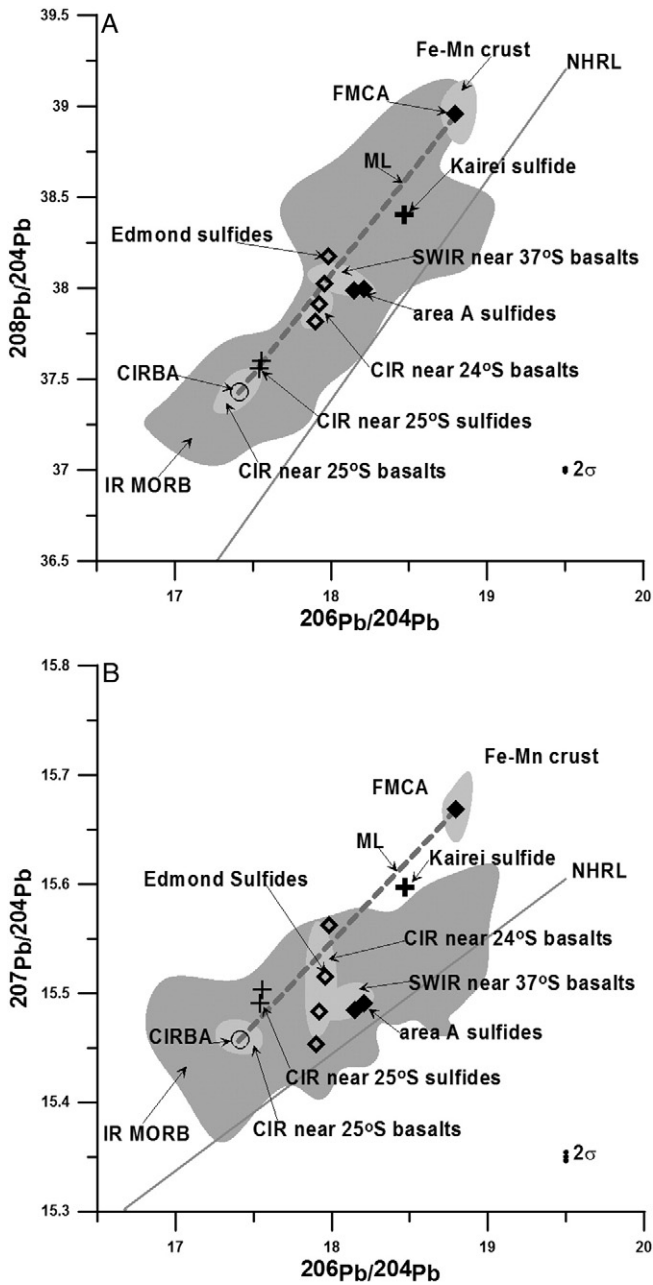
Fig. 6. A: $^{208}Pb/^{204}Pb$ vs. $^{206}Pb/^{204}Pb$; B: $^{207}Pb/^{204}Pb$ vs. $^{206}Pb/^{204}Pb$ plots for hydrothermal sulfides from Edmond hydrothermal field, Kairei hydrothermal field, CIR near 25°S, and area A on the SWIR. The data for CIR near 24°S basalts, CIR near 25°S basalt, SWIR near 37°S basalts, and IR MORB are from the updated PetDB database (http://www.petdb.org). Fe-Mn crust data are from Von Blanckenburg et al. (1996) and Vlastélic et al. (2001). FMCA is average value of Pb isotope ratios in Fe-Mn crust. CIRBA is average value of Pb isotope ratios in CIR near 25°S basalts. ML is mixing line between Pb isotope compositions of FMCA and CIRBA. NHRL is Northern Hemisphere Reference Line (Hart, 1984). Maximum 2σ error for all sulfide samples is also plotted.

Fig. 7. A: $^{208}Pb/^{204}Pb$ vs. $^{206}Pb/^{204}Pb$; B: $^{207}Pb/^{204}Pb$ vs. $^{206}Pb/^{204}Pb$ plots for hydrothermal sulfides from S99HF. Fe-Mn crust data are from Von Blanckenburg et al. (1996). NHRL is Northern Hemisphere Reference Line (Hart, 1984). North Fiji Basin basalts data are from Kim et al. (2006). Maximum 2σ error for all sulfide samples is also plotted.

residence time of fluids. On the sediment-hosted mid-ocean ridges, the Pb of sulfides may be from three sources: sediment, seawater and volcanic rocks. The Pb isotope ratios of sulfides on such ridges (e.g., Middle Valley, Escanaba Trough) have a larger range than those of sulfides from the sediment-starved mid-ocean ridges (e.g., EPR at 1–2°S, EPR at 17°26′S, EPR at 18°31′S; Table 5), and the Pb of sulfides from the sediment-starved mid-ocean ridges is mainly from basaltic rocks. Furthermore, sulfides display significant variations in Pb isotope compositions, such as those from the S99HF. It is likely that hydrothermal fluids percolated through very heterogeneous volcanic sequences

formed of both enriched and depleted MORBs, confirming the results of previous studies by Kim et al. (2006).

For the difference in Pb isotope composition for sulfides from the same hydrothermal field, such as in the EHF and LHF (Table 4), a possible explanation is that it has implications for the residence time of subsurface hydrothermal fluid. These variations could be related to different sulfide ages, and it is regrettable that there are no age data for sulfides from the EHF. The age differences of sulfides from the LHF (3900–60,000 years) (Lalou et al., 1996; Kuznetsov et al., 2006) are insufficient to cause a measurable radiogenic enrichment. We interpret the variations to be a reflection of differences in residence time of subsurface hydrothermal fluid. In the EHF, there is no evidence to show that a sediment component will lead to hydrothermal fluid and related sulfides that have more radiogenic Pb than found in the present study. Furthermore, it is possible that the initial hydrothermal fluid had
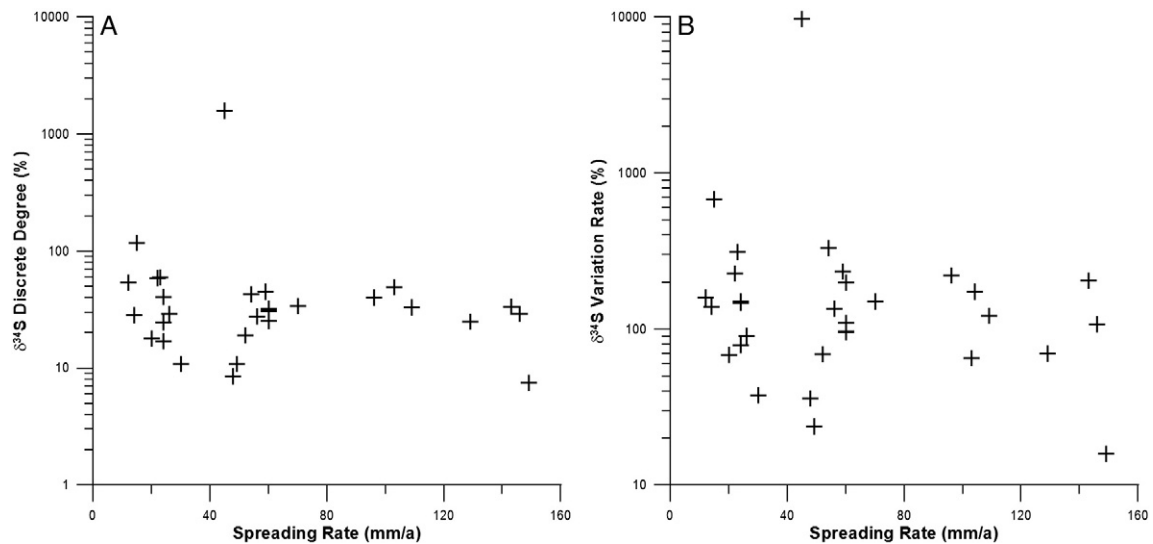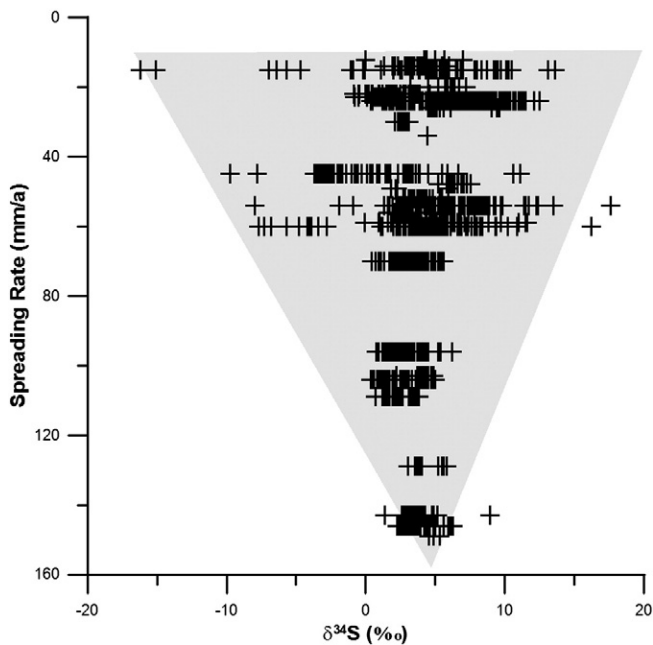
Fig. 8. A: $\delta^{34}S$ discrete degree vs. spreading rate; B: $\delta^{34}S$ variation vs. spreading rate plots for hydrothermal sulfides from different seafloor hydrothermal systems. Sources of sulfur isotope data in sulfides are in Table 2 and references are in Table 3.

different Pb isotope compositions compared with the recently vented hydrothermal fluid because vent fluid evolution is different in different parts of the same hydrothermal field (Yao et al., 2009). Another possible explanation is changing Pb isotope compositions in the hydrothermal fluids. In general, the changes in fluid paths caused by a magmatic/diking event may lead to changes in the chemistry of hydrothermal fluid (Rubin et al., 1994; Von Damm et al., 1995; Fornari et al., 1998; Seyfried et al., 2003). Unfortunately, time- series of Pb isotopic ratios of hydrothermal fluids were not determined in the EHF, and will be the main objective of future studies.

6. Conclusion

The $\delta^{34}S$ values of sulfide minerals from the EPR near 13°N, 11°N, and 1–2°S, LHF, MAR near 13°S, KHF, EHF, CIR near 25°S, area A, and

S99HF vary from 0.0 to 9.6‰, with a mean of 4.7‰, and fall within the $\delta^{34}S$ value range for sulfide samples (n = 1841) from the other seafloor hydrothermal field (1 to 9‰). The $\delta^{34}S$ values are between those of the seawater and the igneous rocks, such as basalt, serpentinized peridotite, and mafic material, suggesting that the S in the sulfide samples is a mixture of that derived from igneous rocks and seawater, but mainly leached from igneous rocks. In the area A, the $\delta^{34}S$ values of pyrite minerals exhibit a larger variation range (from 0.0 to 7.0‰), suggesting that the pyrite minerals are formed by multi-stage hydrothermal fluids. In addition, on the EPR near 1–2°S, EHF, and S99HF, not one of the five measured pyrite–sphalerite pairs, or four measured pyrite–chalcopyrite pairs falls within the range of equilibrium temperatures.

Fig. 9. Plots of $\delta^{34}S$ vs. spreading rate for hydrothermal sulfides from different seafloor hydrothermal systems. Sources of sulfur isotope data in sulfides are in Table 2 and references are in Table 3.
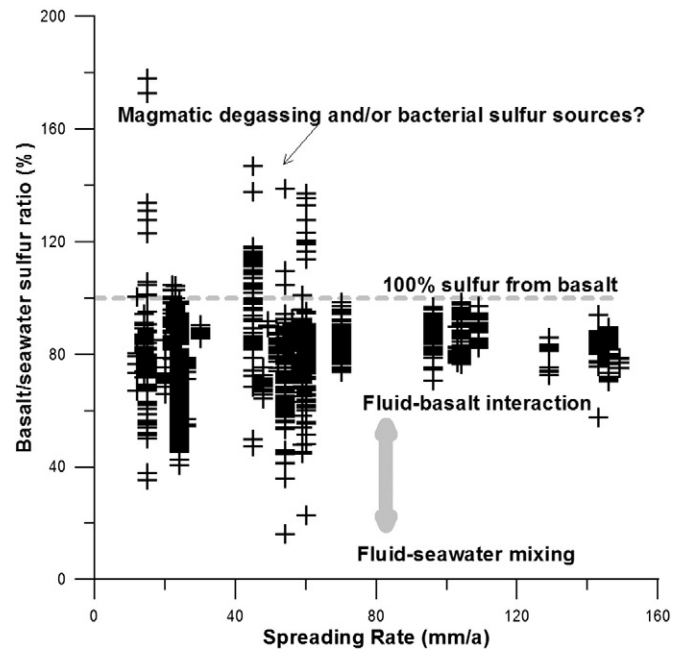
Fig. 10. Basalt/seawater sulfur ratio vs. spreading rate plots for hydrothermal sulfides from different seafloor hydrothermal systems. Basalt/seawater sulfur ratio (%) = $(\delta^{34}S_{seawater} - \delta^{34}S_s) / (\delta^{34}S_{seawater} - \delta^{34}S_{basalt})$, where $\delta^{34}S_{seawater} = 21‰$ (Rees et al., 1978), $\delta^{34}S_{basalt} = 0.1‰$ (Sakai et al., 1984), and $\delta^{34}S_s$ is sulfur isotope ratios in sulfide samples from different seafloor hydrothermal systems. Sources of sulfur isotope data in sulfides are in Table 2 and references are in Table 3.

The Pb isotopic compositions of seafloor hydrothermal sulfides from the EPR near 13°N and 1–2°S, MAR near 13°S, EHF, CIR near 25°S, area A, and S99HF were very homogenous and defined a narrow range, falling in the field of the large Pb isotopic dataset from the EPR, MAR, IR, and NFB basalts, respectively, suggesting that the Pb in the sulfides is derived predominantly from basaltic rocks. In addition, the variations in the S and Pb isotopic compositions of sulfides can be studied using the discrete degree and variation rate, and the variation in the S and Pb isotope compositions of sulfides from deep-sea hydrothermal systems is controlled by the sulfur and lead sources, in combination with the fluid processes including fluid–rock interaction, fluid–seawater mixing and residence time of subsurface hydrothermal fluid.

Acknowledgements

References

Allègre, C.J., Hamelin, B., Dupre, B., 1984. Statistical analysis of isotopic ratios of MORB: the mantle blob cluster model and the convective regime of the mantle. Earth Planet. Sci. Lett. 71, 71–84.

Alt, J.C., Anderson, T.F., 1991. Mineralogy and isotopic composition of sulfur in Layer 3 gabbros from the Indian Ocean, Hole 735B. Proc. Ocean Drill. Program Sci. Results 118, 113–124.

Alt, J.C., Shanks, W.C., 2003. Serpentinization of abyssal peridotites from the MARK area, Mid-Atlantic Ridge: sulfur geochemistry and reaction modeling. Geochim. Cosmochim. Acta 67, 641–653.

Alt, J.C., Anderson, T.F., Bonnell, L., 1989. The geochemistry of sulfur in a 1.3 km section of hydrothermally altered oceanic crust, DSDP Hole 504B. Geochim. Cosmochim. Acta 53, 1011–1023.

Alt, J.C., Shanks, W.C.I.I.I., Bach, W., Paulick, H., Garrido, C.J., Beaudoin, G., 2007. Hydrothermal alteration and microbial sulfate reduction in peridotite and gabbro exposed by detachment faulting at the Mid-Atlantic Ridge, 15°20′N (ODP Leg 209): a sulfur and oxygen isotope study. Geochem. Geophys. Geosyst. 8, Q08002. http://dx.doi.org/10.1029/2007GC001617.

Andrieu, A.-S., Honnorez, J.J., Lancelot, J., 1998. 8. Lead isotope compositions of the TAG mineralization, Mid-Atlantic Ridge, 26°08′N. Proc. Ocean Drill. Program Sci. Results 158, 101–109.

Aoyama, S., Nishizawa, M., Takai, K., Ueno, Y., 2014. Microbial sulfate reduction within the Iheya North subseafloor hydrothermal system constrained by quadruple sulfur isotopes. Earth Planet. Sci. Lett. 398, 113–126.

Arnold, M., Sheppard, S.M.F., 1981. East Pacific Rise at latitude 21°N: isotopic composition and origin of the hydrothermal sulphur. Earth Planet. Sci. Lett. 56, 148–156.

Ben Othman, D., White, W.M., Patchett, J., 1989. The geochemistry of marine sediments, island-arc magma genesis, and crust-mantle recycling. Earth Planet. Sci. Lett. 94, 1–21.

Bjerkgård, T., Cousens, B.L., Franklin, J.M., 2000. The Middle Valley sulfide deposits, northern Juan de Fuca Ridge: radiogenic isotope systematics. Econ. Geol. 95, 1473–1488.

Blum, N., Puchelt, H., 1991. Sedimentary-hosted polymetallic massive sulfide deposits of the Kebrit and Shaban Deeps, Red Sea. Mineral. Deposita 26, 217–227.

Bluth, G.J., Ohmoto, H., 1988. Sulfide-sulfate chimneys on the East Pacific Rise, 11° and 13°N latitude part II: sulfur isotopes. Can. Mineral. 26, 505–515.

Bogdanov, Y.A., Bortnikov, N.S., Vikentyev, I.V., Gurvich, G.S., Sagalevich, A.M., 1997. A new type of modern mineral-forming systems: black smokers of the hydrothermal field at 14°45′N latitude, Mid-Atlantic Ridge. Geol. Ore Deposits 39, 68–90.

Böhlke, J.K., Shanks, W.C.I.I.I., 1994. Stable isotope study of hydrothermal vents at Escanaba trough: observed and calculated effects of sediment-seawater interaction. U.S. Geol. Surv. Bull. 2022, 223–239.

Bowers, T.S., Campbell, A.C., Measures, C.I., Spivack, A.J., Khadem, M., Edmond, J.M., 1988. Chemical controls on the composition of vent fluids at 13°-11°N and 21°N, East Pacific Rise. J. Geophys. Res. 93, 4522–4536.

Brévart, O., Dupré, B., Allègre, C.J., 1981. Metallogenesis at spreading centers: lead isotope systematics for sulfides, manganese-rich crusts, basalts, and sediments from the Cyamex and Alvin areas (East Pacific Rise). Econ. Geol. 76, 1205–1210.

Brunner, B., Bernasconi, S.M., 2005. A revised isotope fractionation model for dissimilatory sulfate reduction in sulfate reducing bacteria. Geochim. Cosmochim. Acta 69, 4759–4771.

Butler, I.B., Fallick, A.E., Nesbitt, R.W., 1998. Mineralogy, sulphur isotope geochemistry and the development of sulphide structures at the Broken Spur hydrothermal vent site, 29°10′N Mid-Atlantic Ridge. J. Geol. Soc. Lond. 155, 773–785.

Butterfield, D.A., Massoth, G.J., McDuff, R.E., Lupton, J.E., Lilley, M.D., 1990. Geochemistry of hydrothermal fluids from Axial Seamount Hydrothermal Emissions Study vent field, Juan de Fuca Ridge; subseafloor boiling and subsequent fluid-rock interaction. J. Geophys. Res. 95, 12895–12921.

Campbell, A.C., Bowers, T.S., Measures, C.I., Falkner, K.K., Khadem, M., Edmond, J.M., 1988. A time-series of vent fluid compositions from 21°N East Pacific Rise (1979, 1981, 1985) and the Guaymas Basin, Gulf of California (1982, 1985). J. Geophys. Res. 93, 4537–4549.

Charlou, J.L., Donval, J.P., Fouquet, Y., Jean-Baptiste, P., Holm, N., 2002. Geochemistry of high H2 and CH4 vent fluids issuing from ultramafic rocks at the Rainbow hydrothermal field (36°14′N, MAR). Chem. Geol. 191, 345–359.

Chen, J., 1987. U, Th and Pb isotopes in hot springs on the Juan de Fuca Ridge. J. Geophys. Res. 92, 11411–11415.

Chiba, H., Uchiyama, N., Teagle, D.A.H., 1998. Stable isotope study of anhydrite and sulfide minerals at the TAG hydrothermal mound, Mid-Atlantic Ridge, 26°N. Proc. Ocean Drill. Program Sci. Results 158, 85–90.

Church, S.E., Tatsumoto, M., 1975. Lead isotopic relations in oceanic ridge basalts from the Juan de Fuca-Gorda Ridge area, N.E. Pacific Ocean. Contrib. Mineral. Petrol. 53, 253–279.

Cousens, B.L., Allan, J.F., Leybourne, M.I., Chase, R.L., Van Wagoner, N., 1995. Mixing of magmas from enriched and depleted mantle sources in the northeast Pacific: West Valley segment, Juan de Fuca Ridge. Contrib. Mineral. Petrol. 120, 337–357.

Cousens, B.L., Blenkinsop, J., Franklin, J.M., 2002. Lead isotope systematics of sulfide minerals in the Middle Valley hydrothermal system, northern Juan de Fuca Ridge. Geochem. Geophys. Geosyst. 3 (5). http://dx.doi.org/10.1029/2001GC000257.

Crowe, D.E., Valley, J.W., 1992. Laser microprobe study of sulphur isotope variation in a sea-floor hydrothermal spire, Axial Seamount, Juan de Fuca Ridge, eastern Pacific. Chem. Geol. 101, 63–70.

de Ronde, C., Faure, K., Bray, C.M., Chappell, D.A., Wright, I.C., 2003. Hydrothermal fluids associated with seafloor mineralization at two southern Kermadec arc volcanoes, offshore New Zealand. Mineral. Deposita 38, 217–233.

Delacour, A., Früh-Green, G.L., Bernasconi, S.M., Kelley, D.S., 2008. Sulfur in peridotites and gabbros at Lost City (30°N, MAR): implications for hydrothermal alteration and microbial activity during serpentinization. Geochim. Cosmochim. Acta 72, 5090–5110.

Duckworth, R.C., Fallick, A.E., Rickard, D., 1994. Mineralogy and sulfur isotopic composition of the Middle Valley massive sulfide deposit, northern Juan de Fuca Ridge. Proc. Ocean Drill. Program Sci. Results 139, 373–385.

Duckworth, R.C., Knott, R., Fallick, A.E., Rickard, D., Murton, B.J., van Dover, C., 1995. Mineralogy and sulphur isotope geochemistry of the Broken Spur sulphides, 29°N Mid-Atlantic Ridge. Geol. Soc. Lond. Spec. Publ. 87, 175–189.

Eissen, J.P., Nohara, M., Cotten, J., Hirose, K., 1994. North Fiji Basin basalts and their magma sources: part I. Incompatible element constraints. Mar. Geol. 116, 153–178.

Farquhar, J., Johnston, D.T., Wing, B.A., Habicht, K.S., Canfield, D.E., Airieau, S., Thiemens, M.H., 2003. Multiple sulphur isotopic interpretations of biosynthetic pathways: implications for biological signatures in the sulphur isotope record. Geobiology 1, 27–36.

Fornari, D.J., Shank, T., Von Damm, K.L., Gregg, T.K.P., Lilley, M., Levai, G., Bray, A., Haymon, R.M., Perfit, M.R., Lutz, R., 1998. Time-series temperature measurements at high-temperature hydrothermal vents, East Pacific Rise 9°49′–51′N: evidence for monitoring a crustal cracking event. Earth Planet. Sci. Lett. 160, 419–431.

Fouquet, Y., Marcoux, E., 1995. Lead isotope systematics in Pacific hydrothermal sulfide deposits. J. Geophys. Res. 100 (B4), 6025–6040.

Fouquet, Y., Knott, R., Cambon, P., Fallick, A.E., Rickard, D., Desbruyeres, D., 1996. Formation of large sulfide mineral deposits along fast spreading ridges: examples from

off-axial deposits at 12°43′N on the East Pacific Rise. Earth Planet. Sci. Lett. 144, 147–162.

Gemmell, J.B., Sharpe, R., 1998. Detailed sulfur-isotope investigation of the TAG hydrothermal mound and stockwork zone. Proc. Ocean Drill. Program Sci. Results 158, 71–84.

Gemmell, J.B., Sharpe, R., Jonasson, I.R., Herzig, P.M., 2004. Sulfur isotope evidence for magmatic contributions to submarine and subaerial gold mineralization: conical Seamount and the Ladolam gold deposit, Papua New Guinea. Econ. Geol. 99, 1711–1725.

German, C.R., Barreiro, B.A., Higgs, N.C., Nelsen, T.A., Ludford, E.M., Palmer, M.R., 1995. Seawater-metasomatism in hydrothermal sediments (Escanaba Trough, northeast Pacific). Chem. Geol. 119, 175–190.

Goldhaber, M.B., Kaplan, I.R., 1980. Mechanisms of sulfur incorporation and isotope fractionation during early diagenesis in sediments of the Gulf of California. Mar. Chem. 9, 95–143.

Goodfellow, W.D., Franklin, J.M., 1993. Geology, mineralogy, and chemistry of sediment-hosted clastic massive sulfides in shallow cores, Middle Valley, northern Juan de Fuca Ridge. Econ. Geol. 88, 2037–2068.

Halbach, P., Münch, U., 2000. Mineral deposits at 23°S, Central Indian Ridge: mineralogical features, chemical composition, and isotopic investigations. In: Cronan, D.S. (Ed.), Handbook of Marine Mineral Deposits. CRC Press, Boca Rotan, FL, pp. 327–346.

Halbach, P., Nakamura, K., Wahsner, M., Lange, J., Sakai, H., Käselitz, L., Hansen, R.D., Yamano, M., Post, J., Prause, B., Seifert, R., Michaelis, W., Teichmann, F., Kinoshita, M., Märten, A., Ishibashi, J., Czerwinski, S., Blum, N., 1989. Probable modern analogue of Kuroko-type massive sulphide deposits in the Okinawa Trough back-arc basin. Nature 338, 496–499.

Halbach, P., Hansmann, W., Koppel, V., Pracejus, B., 1997. Whole-rock and sulfide lead-isotope data from the hydrothermal JADE field in the Okinawa back-arc trough. Mineral. Deposita 32, 70–78.

Hamelin, B., Dupré, B., Allègre, C.J., 1984. Lead-strontium isotopic variations along the East Pacific Rise and the Mid-Atlantic Ridge: a comparative study. Earth Planet. Sci. Lett. 67, 340–350.

Hannington, M.D., Scott, S.D., 1988. Mineralogy and geochemistry of an hydrothermal silica-sulfide-sulfate spire in the caldera of Axial Seamount, Juan de Fuca Ridge. Can. Mineral. 26, 603–625.

Hannington, M.D., de Ronde, C., Petersen, S., 2005. Sea-floor tectonics and submarine hydrothermal systems. In: Hedenquist, J.W., Thompson, J.F.H., Goldfarb, R.J., Richards, J.P. (Eds.), Econ. Geol. 100th Anniv. Vol., pp. 111–141.

Hart, S.R., 1984. A large scale isotope anomaly in the Southern Hemisphere mantle. Nature 309, 753–757.

Hegner, E., Tatsumoto, M., 1987. Pb, Sr, and Nd isotopes in basalts and sulfides from the Juan de Fuca Ridge. J. Geophys. Res. 92 (B11), 11380–11386.

Hekinian, R., Fevrier, M., Bischoff, J.L., Picot, P., Shanks, W.C., 1980. Sulfide deposits from the East Pacific Rise near 21°N. Science 207, 1433–1444.

Herzig, P.M., Hannington, M.D., Arribas, A., 1998a. Sulfur isotopic composition of hydrothermal precipitates from the Lau back-arc: implications for magmatic contributions to seafloor hydrothermal systems. Mineral. Deposita 33, 226–237.

Herzig, P.M., Petersen, S., Hannington, M.D., 1998b. Geochemistry and sulfur isotopic composition of the TAG hydrothermal mound, Mid-Atlantic Ridge, 26°N. Proc. Ocean Drill. Program Sci. Results 158, 47–70.

Hinkley, T.K., Tatsumoto, M., 1987. Metals and isotopes in Juan de Fuca Ridge hydrothermal fluid and their associated solid materials. J. Geophys. Res. 92, 11400–11410.

Iizasa, K., Yusa, M., Yokota, S., 1992. Mineralogy and geochemistry of volcanogenic sulfides from the Myojinsho submarine caldera, the Sichito-Iwojima Ridge, Izu-Ogasawara arc, northwestern Pacific. Mar. Geol. 108, 39–58.

Kase, K., Yamamoto, M., Shibata, T., 1990. Copper-rich sulfide deposits near 23°N, Mid-Atlantic Ridge: chemical composition, mineral chemistry, and sulfur isotopes. Proc. Ocean Drill. Program Sci. Results 106 (109), 163–172.

Kerridge, J.F., Haymon, R.M., Kastner, M., 1983. Sulfur isotope systematics at the 21°N site, East Pacific Rise. Earth Planet. Sci. Lett. 66, 91–100.

Kim, J., Lee, I., Lee, K.-Y., 2004. S, Sr, and Pb isotopic systematics of hydrothermal chimney precipitates from the Eastern Manus Basin, western Pacific: evaluation of magmatic contribution to hydrothermal system. J. Geophys. Res. 109, B12210. http://dx.doi.org/10.1029/2003JB002912.

Kim, J., Lee, I., Halbach, P., Lee, K.-Y., Ko, Y.-T., Kim, K.-H., 2006. Formation of hydrothermal vents in the North Fiji Basin: sulfur and lead isotope constraints. Chem. Geol. 233, 257–275.

Knott, R., Fallick, A.E., Rickard, D., Bäcker, H., 1995. Mineralogy and Sulphur isotope characteristics of a massive sulphide boulder, Galapagos Rift, 85°55′W. Geol. Soc. Lond. Spec. Publ. 87, 207–222.

Knott, R., Fouquet, Y., Honnorez, J., Petersen, S., Bohn, M., 1998. Petrology of hydrothermal mineralization: a vertical section through the TAG mound. Proc. Ocean Drill. Program Sci. Results 158, 5–26.

Koschinsky, A., Seifert, R., Halbach, P., Bau, M., Brasse, S., de Carvalho, L.M., Fonseca, N.M., 2002. Geochemistry of diffuse low-temperature hydrothermal fluids in the North Fiji Basin. Geochim. Cosmochim. Acta 66, 1409–1427.

Koski, R.A., Lonsdale, P.F., Shanks, W.C.I.I.I., Berndt, M.E., Howe, S.S., 1985. Mineralogy and geochemistry of a sediment-hosted hydrothermal sulfide deposit from the southern trough of Guaymas Basin, Gulf of California. J. Geophys. Res. 90, 6695–6707.

Koski, R.A., Shanks, W.C.I.I.I., Bohrson, W.A., Oscarson, R.L., 1988. The composition of massive sulfide deposits from the sediment-covered floor of Escanaba trough, Gorda Ridge: implications for depositional processes. Can. Mineral. 26, 655–673.

Kumagai, H., Nakamura, K., Toki, T., Morishita, T., Okino, K., Ishibashi, J.–.I., Tsunogai, U., Kawagucci, S., Gamo, T., Shibuya, T., Sawaguchi, T., Neo, N., Joshima, M., Sato, T., Takai, K., 2008. Geological background of the Kairei and Edmond hydrothermal fields along the Central Indian Ridge: implications of their vent fluids' distinct chemistry. Geofluids 8, 239–251.

Kusakabe, M., Mayeda, S., Nakamura, E., 1990. S, O and Sr isotope systematics of active vent materials from the Mariana backarc basin spreading axis at 18°N. Earth Planet. Sci. Lett. 100, 275–282.

Kuznetsov, V., Cherkashev, G., Lein, A., Shilov, V., Maksimov, F., Arslanov, K., Stepanova, T., Baranova, N., Chernov, S., Tarasenko, D., 2006. 230Th/U dating of massive sulfides from the Logatchev and Rainbow hydrothermal fields (Mid-Atlantic Ridge). Geochronometria 25, 51–55.

Lalou, C., Reyss, J.L., Brichet, E., Krasnov, S., Stepanova, T., Cherkashev, G., Markov, V., 1996. Initial chronology of a recently discovered hydrothermal field at 14°45′N, Mid-Atlantic Ridge. Earth Planet. Sci. Lett. 144, 483–490.

LeHuray, A.P., Church, S.E., Koski, R.A., Bouse, R.M., 1988. Pb isotopes in sulfides from mid-ocean ridge hydrothermal sites. Geology 16, 362–365.

Lein, A.Y., Ulyanova, N.V., Grinenko, V.A., Lisitsyn, A.P., 1991. Geochemistry of the hydrothermal sulfide ores of the Mid-Atlantic Ridge (26°N). Geochem. Int. 28, 1–13.

Lein, A.Y., Ulyanova, N.V., Grinenko, V.A., Bibikova, Y.V., Lisitsyn, A.P., 1993. Mineralogical and geochemical features of the Manus basin hydrothermal sulfide ores, Bismarck Sea. Geochem. Int. 30, 57–71.

Lein, A.Y., Ulyanova, N.V., Ulyanov, A.A., Cherkashev, G.A., Stepanova, T.V., 2001. Mineralogy and geochemistry of sulfide ores in ocean-floor hydrothermal fields associated with serpentinite protrusions. Russ. J. Earth Sci. 3, 371–393.

Marchig, V., Blum, N., Roonwal, G., 1997. Massive sulfide chimneys from the East Pacific Rise at 7°24′S and 16°43′S. Mar. Georesour. Geotechnol. 15, 49–66.

Marumo, K., Hattori, K.H., 1999. Seafloor hydrothermal clay alteration at Jade in the back-arc Okinawa Trough: mineralogy, geochemistry and isotope characteristics. Geochim. Cosmochim. Acta 63, 2785–2804.

Massoth, G.J., Butterfield, D.A., Lupton, J.E., McDuff, R.E., Lilley, M.D., Jonasson, I.R., 1989. Submarine venting of phase-separated hydrothermal fluids at Axial Volcano, Juan de Fuca Ridge. Nature 340, 702–705.

McConachy, T.F., 1988. Hydrothermal Plumes and Related Deposits Over Spreading Ridges in the Northeast Pacific Ocean: The East Pacific Rise Near 11°N and 21°N, Explorer Ridge, and the J. Tuzo Wilson Seamounts. (Unpubl. Ph.D. Thesis). University of Toronto, Toronto, ON (403 pp).

McDermott, J.M., Ono, S., Tivey, M.K., Seewald, J.S., Shanks III, W.C., Solow, A.R., 2015. Identification of sulfur sources and isotopic equilibria in submarine hot-springs using multiple sulfur isotopes. Geochim. Cosmochim. Acta 160, 169–187.

Merlivat, L., Pineau, F., Javoy, M., 1987. Hydrothermal vent waters at 13°N on the East Pacific Rise: isotopic composition and gas concentration. Earth Planet. Sci. Lett. 84, 100–108.

Michard, G., Albarède, F., Michard, A., Minster, J.-F., Charlou, J.-J., Tan, N., 1984. Chemistry of solutions from the 13°N East Pacific Rise hydrothermal site. Earth Planet. Sci. Lett. 67:297–307. http://dx.doi.org/10.1016/0012-821X(84)90169-9.

Mottl, M.J., Holland, H.D., Corr, R.F., 1979. Chemical exchange during hydrothermal alteration of basalt by seawater. II. Experimental results for Fe, Mn, and sulfur species. Geochim. Cosmochim. Acta 43, 869–884.

Nakamura, K., Morishita, T., Bach, W., Klein, F., Hara, K., Okino, K., Takai, K., Kumagai, H., 2009. Serpentinized troctolites exposed near the Kairei hydrothermal field, Central Indian Ridge: insights into the origin of the Kairei hydrothermal fluid supporting a unique microbial ecosystem. Earth Planet. Sci. Lett. 280, 128–136.

Nohara, M., Hirose, K., Eissen, J.P., Urabe, T., Joshima, M., 1994. The North Fiji Basin basalts and their magma sources: part II. Sr–Nd isotopic and trace element constraints. Mar. Geol. 116, 179–195.

Ohmoto, H., 1986. Stable isotope geochemistry of ore deposits. Rev. Mineral. Geochem. 16 (1), 491–560.

Ohmoto, H., Goldhaber, M., 1997. Sulfur and carbon isotopes. In: Barnes, H.L. (Ed.), Geochemistry of Hydrothermal Ore Deposits, 3rd ed. J. Wiley and Sons, New York, pp. 517–612.

Ohmoto, H., Lasaga, A.C., 1982. Kinetics of reactions between aqueous sulfates and sulfides in hydrothermal systems. Geochim. Cosmochim. Acta 46, 1727–1745.

Ohmoto, H., Rye, R.O., 1979. Isotopes of sulfur and carbon. In: Barnes, H.L. (Ed.), Geochemistry of Hydrothermal Ore Deposits, 2nd ed. J. Wiley and Sons, New York, pp. 509–567.

Ohmoto, H., Mizukami, M., Drummond, S.E., Eldridge, C.S., Pisutha-Arnond, V., Lenagh, T.C., 1983. Chemical processes of Kuroko formation. Econ. Geol. Monogr. 5, 570–604.

Ono, S., Wing, B.A., Johnston, D., Farquhar, J., Rumble, D., 2006. Mass-dependent fractionation of quadruple sulfur isotope system as a new tracer of sulfur biogeochemical cycles. Geochim. Cosmochim. Acta 70, 2238–2252.

Ono, S., Shanks, W.C.I.I.I., Rouxel, O.J., Rumble, D., 2007. S-33 constraints on the seawater sulfate contribution in modern seafloor hydrothermal vent sulfides. Geochim. Cosmochim. Acta 71, 1170–1182.

Peter, J.M., Shanks, W.C., 1992. Sulfur, carbon, and oxygen isotope variations in submarine hydrothermal deposits of Guaymas basin, Gulf of California, USA. Geochim. Cosmochim. Acta 56, 2025–2040.

Petersen, S., Herzig, P.M., Hannington, M.D., Jonasson, I.R., Arribas Jr., A., 2002. Submarine vein-type gold mineralization near Lihir island, New Ireland fore-arc, Papua New Guinea. Econ. Geol. 97, 1795–1813.

Petersen, S., Kuhn, T., Herzig, P.M., Hannington, M.D., 2005. Factors controlling precious and base-metal enrichments at the ultramafic-hosted Logatchev hydrothermal field, 14°45′N on the MAR: new insights from cruise M60/3. In: Mao, J., Bierlein, F.P. (Eds.), Mineral Deposit Research: Meeting the Global Challenge. Proceedings of the 8th Biennial SGA Meeting Beijing, China, pp. 679–682.

Petersen, S., Kuhn, K., Kuhn, T., Augustin, N., Hékinian, R., Franz, L., Borowski, C., 2009. The geological setting of the ultramafic-hosted Logatchev hydrothermal field (14°45′N, Mid-Atlantic Ridge) and its influence on massive sulfide formation. Lithos 112, 40–56.

Rees, C.E., Jenkins, W.J., Monster, J., 1978. The sulphur isotopic composition of ocean water sulphate. Geochim. Cosmochim. Acta 42, 377–381.

Rouxel, O., Fouquet, Y., Ludden, J.N., 2004a. Subsurface processes at the Lucky Strike hydrothermal field, Mid-Atlantic Ridge: evidence from sulfur, selenium and iron isotopes. Geochim. Cosmochim. Acta 68, 2295–2311.

Rouxel, O., Fouquet, Y., Ludden, J.N., 2004b. Copper isotope systematics of the Lucky Strike, Rainbow and Logatchev seafloor hydrothermal fields on the Mid Atlantic Ridge. Econ. Geol. 99, 585–600.

Rouxel, O., Shanks, W.C.I.I.I., Bach, W., Edwards, K.J., 2008. Integrated Fe- and S-isotope study of seafloor hydrothermal vents at East Pacific Rise 9–10°N. Chem. Geol. 252, 214–227.

Rubin, K.H., Macdougall, J.D., Perfit, M.R., 1994. $^{210}Po/^{210}Pb$ dating of recent volcanic eruptions on the sea floor. Nature 368, 841–844.

Sakai, H., Des Marais, D.J., Ueda, A., Moore, J.G., 1984. Concentrations and isotope ratios of carbon, nitrogen and sulfur in ocean-floor basalts. Geochim. Cosmochim. Acta 48, 2433–2441.

Seal, R.R.I.I., 2006. Sulfur isotope geochemistry of sulfide minerals. Rev. Mineral. Geochem. 61, 633–677.

Seal, R.R.I.I., Rye, R.O., Alpers, C.N., 2000. Stable isotope systematics of sulfate minerals. Rev. Mineral. Geochem. 40, 541–602.

Seyfried, W.E., Seewald, J.S., Berndt, M.E., Ding, K., Foustoukos, D.I., 2003. Chemistry of hydrothermal vent fluids from the Main Endeavour Field, northern Juan de Fuca Ridge: geochemical controls in the aftermath of June 1999 seismic events. J. Geophys. Res. 108. http://dx.doi.org/10.1029/2002JB001957.

Shanks, W.C.I.I.I., 2001. Stable isotope in seafloor hydrothermal systems: vent fluids, hydrothermal deposits, hydrothermal alteration, and microbial processes. Rev. Mineral. Geochem. 43, 469–525.

Shanks, W.C.I.I.I., Bischoff, J.L., 1977. Ore transport and deposition in the Red Sea geothermal system: a geochemical model. Geochim. Cosmochim. Acta 41, 1507–1519.

Shanks, W.C.I.I.I., Bischoff, J.L., 1980. Geochemistry, sulfur isotope composition, and accumulation rates of Red Sea geothermal deposits. Econ. Geol. 74, 445–459.

Shanks, W.C.I.I.I., Niemitz, J., 1982. Sulfur isotope studies of hydrothermal anhydrite and pyrite, Deep Sea Drilling Project Leg 64, Guaymas Basin, Gulf of California. Initial Rep. Deep Sea Drill. Proj. 64, 1137–1142.

Shanks, W.C.I.I.I., Seyfried Jr., W.E., 1987. Stable isotope studies of vent fluids and chimney minerals, southern Juan de Fuca Ridge: sodium metasomatism and seawater sulfate reduction. J. Geophys. Res. 92, 11387–11399.

Shanks, W.C.I.I.I., Bischoff, J.L., Rosenbauer, R.J., 1981. Seawater sulfate reduction and sulfur isotope fractionation in basaltic systems: interaction of seawater with fayalite and magnetite at 200–350 °C. Geochim. Cosmochim. Acta 45, 1977–1995.

Shanks, W.C.I.I.I., Bohlke, J.K., Seal, R.R.I.I., 1995. Stable isotopes in mid-ocean ridge hydrothermal systems: interactions between fluids, minerals, and organisms. In: Humphris, S.E., Zierenberg, R.A., Mullineaux, L.S., Thomson, R.E. (Eds.), Seafloor Hydrothermal Systems: Physical, Chemical, Biological, and Geological InteractionsGeophys. Monogr. Ser. vol. 91. Amer. Geophys. Union, pp. 194–221.

Smith, J.W., Doolan, S., McFarlane, E.F., 1977. A sulfur isotope geothermometer for the trisulfide system galena-sphalerite-pyrite. Chem. Geol. 19, 83–90.

Solomon, M., Eastoe, C.J., Walshe, J.L., Green, G.R., 1988. Mineral deposits and sulfur isotope abundances in the Mount Read Volcanics between Que River and Mount Darwin, Tasmania. Econ. Geol. 83, 1307–1328.

Stepanova, T.V., Krasnov, S.G., Cherkashev, G.A., 1996. Mineralogy, chemical composition and structure of the MIR mound, TAG hydrothermal field. Geophys. Res. Lett. 23, 3515–3518.

Stuart, F.M., Turner, G., Duckworth, R.C., Fallick, A.E., 1994a. Helium isotopes as tracers of trapped hydrothermal fluids in ocean-floor sulfides. Geology 22, 823–826.

Stuart, F.M., Duckworth, R., Turner, G., Schofield, P.F., 1994b. Helium and sulfur isotopes of sulfide minerals from Middle Valley, northern Juan de Fuca Ridge. Proc. Ocean Drill. Program Sci. Results 139, 387–392.

Stuart, F.M., Harrop, P.J., Knott, R., Fallick, A.E., Turner, G., Fouquet, Y., Rickard, D., 1995. Noble gas isotopes in 25000 years of hydrothermal fluids from 13°N on the East Pacific Rise. Geol. Soc. Lond. Spec. Publ. 87, 133–143.

Stuart, F.M., Ellam, R.M., Duckworth, R.C., 1999. Metal sources in the Middle Valley massive sulphide deposit, northern Juan de Fuca Ridge: Pb isotope constraints. Chem. Geol. 153, 213–225.

Styrt, M.M., Brackmann, A.J., Holland, H.D., Clark, B.C., Pisutha-Arnond, V., Eldridge, C.S., Ohmoto, H., 1981. The mineralogy and the isotopic composition of sulfur in hydrothermal sulfide/sulfate deposits on the East Pacific Rise, 21°N latitude. Earth Planet. Sci. Lett. 53, 382–390.

Sun, S.S., 1980. Lead isotopic studies of young volcanic rocks from oceanic islands, mid-oceanic ridge and island arcs. Philos. Trans. R. Soc Lond. A 297, 409–445.

Tatsumoto, M., 1978. Isotopic composition of lead in oceanic basalt and its implication to mantle evolution. Earth Planet. Sci. Lett. 38, 63–87.

Verati, C., Lancelot, J., Hékinian, R., 1999. Pb isotope study of black-smokers and basalts from Pito Seamount site (Easter microplate). Chem. Geol. 155, 45–63.

Vidal, P., Clauer, N., 1981. Pb and Sr isotopic systematics of some basalts and sulfides from the East Pacific Rise at 21°N (project RITA). Earth Planet. Sci. Lett. 55, 237–246.

Vlastélic, I., Abouchami, W., Galer, S.J.G., Hofmann, A.W., 2001. Geographic control on Pb isotope distribution and sources in Indian Ocean Fe-Mn deposits. Geochim. Cosmochim. Acta 65, 4303–4319.

von Blanckenburg, F., O'Nions, R.K., Hein, J.R., 1996. Distribution and sources of pre-anthropogenic lead isotopes in deep ocean water from Fe-Mn crusts. Geochim. Cosmochim. Acta 60, 4957–4963.

Von Damm, K.L., Bischoff, J.L., 1987. Chemistry of hydrothermal solutions from the Southern Juan de Fuca Ridge. J. Geophys. Res. 92, 11334–11346.

Von Damm, K.L., Oosting, S.E., Kozlowskl, R., Buttermore, L.G., Colodner, D.C., Edmonds, H.N., Edmond, J.M., Grebmeier, J.M., 1995. Evolution of East Pacific Rise hydrothermal vent fluids following a volcanic eruption. Nature 375, 47–50.

Woodruff, L.G., Shanks, W.C.I.I.I., 1988. Sulfur isotope study of chimney minerals and hydrothermal fluids from 21°N, East Pacific Rise: hydrothermal sulfur sources and disequilibrium sulfate reduction. J. Geophys. Res. 93, 4562–4572.

Yao, H.Q., Zhou, H.Y., Peng, X.T., Bao, S.X., Wu, Z.J., Li, J.T., Sun, Z.L., Chen, Z.Q., Li, J.W., Chen, G.Q., 2009. Metal sources of black smoker chimneys, Endeavour Segment, Juan de Fuca Ridge: Pb isotope constraints. Appl. Geochem. 24, 1971–1977.

Yin, X.B., Zeng, Z.G., Li, S.Z., Wu, L, Wang, X.Y., Zhang, G.L., Chen, S., 2011. Determination of trace elements in sulfide samples by inductively coupled plasma-mass spectrometry. Chin. J. Anal. Chem. 39, 1228–1232 (in Chinese with English abstract).

Zeng, Z.G., Jiang, F.Q., Zhai, S.K., Qin, Y.S., 2000a. Lead isotopic compositions of massive sulfides from the Jade hydrothermal field in the Okinawa Trough and its geological implications. Geochimica 29, 239–245 (in Chinese with English abstract).

Zeng, Z.G., Qin, Y.S., Zhao, Y.Y., Zhai, S.K., 2000b. Sulfur isotopic composition of seafloor surface hydrothermal sediments in the TAG hydrothermal field of Mid-Atlantic Ridge and its geological implications. Oceanol. Limnol. Sin. 31 (5), 518–529 (in Chinese with English abstract).

Zeng, Z.G., Li, J., Jiang, F.Q., Zhai, S.K., Qin, Y.S., Hou, Z.Q., 2002a. Sulfur isotopic composition of seafloor hydrothermal sediment from the Jade hydrothermal field in the central Okinawa Trough and its geological significance. Acta Oceanol. Sin. 21 (3), 395–405.

Zeng, Z.G., Li, J., Jiang, F.Q., Qin, Y.S., Zhai, S.K., 2002b. Sulfur isotopic composition of modern seafloor hydrothermal sediment and its geological significance. Acta Oceanol. Sin. 21 (4), 519–528.

Zeng, Z.G., Chen, D.G., Yin, X.B., Wang, X.Y., Zhang, G.L., Wang, X.M., 2010. Elemental and isotopic compositions of the hydrothermal sulfide on the East Pacific Rise near 13°N. Sci. China Ser. D Earth Sci. 53 (22), 253–266.

Zeng, Z.G., Chen, S., Selby, D., Yin, X.B., Wang, X.Y., 2014. Rhenium-osmium abundance and isotopic compositions of massive sulfides from modern deep-sea hydrothermal systems: implications for vent associated ore forming processes. Earth Planet. Sci. Lett. 396, 223–234.

Zeng, Z.G., Niedermann, S., Chen, S., Wang, X.Y., Li, Z.X., 2015a. Noble gases in sulfide deposits of modern deep-sea hydrothermal systems: implications for heat fluxes and hydrothermal fluid processes. Chem. Geol. 409, 1–11.

Zeng, Z.G., Ma, Y., Yin, X.B., Selby, D., Kong, F.C., Chen, S., 2015b. Factors affecting the rare earth element compositions in massive sulfides from deep-sea hydrothermal systems. Geochem. Geophys. Geosyst. 16:2679–2693. http://dx.doi.org/10.1002/2015GC005812.

Zierenberg, R.A., 1994. Sulfur content of sediments and sulfur isotope values of sulfide and sulfate minerals from Middle Valley. Proc. Ocean Drill. Program Sci. Results 139, 739–748.

Zierenberg, R.A., Shanks, W.C., 1988. Isotopic studies of epigenetic features in metalliferous sediment, Atlantis II Deep, Red Sea. Can. Mineral. 26, 737–753.

Zierenberg, R.A., Shanks, W.C., 1994. Sediment alteration associated with massive sulfide formation in Escanaba trough, Gorda Ridge: the importance of seawater mixing and magnesium metasomatism. U.S. Geol. Surv. Bull. 2022, 257–277.

Zierenberg, R.A., Shanks, W.C., Bischoff, J.L., 1984. Massive sulfide deposits at 21°, East Pacific Rise: chemical composition, stable isotopes, and phase equilibria. Geol. Soc. Am. Bull. 95, 922–929.

Zierenberg, R.A., Koski, R.A., Morton, J.L., Bouse, R.M., Shanks, W.C.I.I.I., 1993. Genesis of massive sulfide deposits on a sediment-covered spreading center, Escanaba trough, southern Gorda Ridge. Econ. Geol. 88, 2069–2098.